Acta Neuropathologica (2026) 151:50
https://doi.org/10.1007/s00401-026-03019-0

ORIGINAL PAPER

Pathogenic IgG from long COVID patients with neurological sequelae triggers sensitive but not cognitive impairments upon transfer into mice

Margaux Mignolet[1] · Catherine Deroux[2] · Thomas Florkin[1] · Valéry Bielarz[1] · Kathleen De Swert[1] · Nicolas Halloin[1] · Lindsay Sprimont[1] · Aurélie Ladang[3] · Fabienne George[4,5] · Jacques Gilloteaux[1,6] · Laurence Abeloos[7] · Pierre Garin[8,9] · Johan Van Weyenbergh[10] · Marc Jamoulle[11] · Claire Diederich[12] · Nicolas Albert Gillet[12] · Pierre Bulpa[5,13] · Charles Nicaise[1]

Received: 28 November 2025 / Revised: 14 April 2026 / Accepted: 15 April 2026

Abstract

Approximately 30% of long COVID patients still experience neurological symptoms (brain fog, pain, chronic fatigue) more than 4 months after the onset of COVID-19. This condition, known as 'neurological long COVID', remains poorly understood and might be explained by a persisting autoimmune response against nervous-derived self-antigens. The aim of this study is to determine whether IgG autoantibodies from long COVID patients with neurological sequelae can bind to central or peripheral nervous system epitopes and trigger neuropsychiatric symptoms upon passive transfer into mice, thereby mirroring patient-reported manifestations. Long COVID patients meeting the 2021 consensus WHO definition were included following a standardized neuropsychological assessment, while excluding patients with a medical history of autoimmune and neurological disorders. Age- and sex-matched asymptomatic individuals were used as healthy controls. Total IgGs were isolated using protein G purification and injected intraperitoneally into C57Bl6/J mice for four consecutive days. During the two weeks post-injections, behavioral tests assessed mechanical allodynia, thermal hyperalgesia, spatial working memory, depression, and anxiety. Mice injected with IgG from long COVID patients showed no difference with the control group in terms of anxiety or depression behaviors, short- or long-term spatial memories. However, they displayed a transient decrease of paw withdrawal threshold and thermal hypersensitivity during the first week. This effect was abolished when IgG-depleted serum or papain-digested IgGs were transferred. IgG from long COVID patients accumulated in the lumbar dorsal root ganglia of injected mice and colocalized with proprioceptive and nociceptive sensory neurons, without inducing local neuroinflammation or astrogliosis. When applied onto human *post-mortem* DRG tissue, patient-derived IgG also exhibited immunoaffinity for sensory neuron somata. These data demonstrate that IgGs from long COVID patients bind to peripheral sensory neurons and induce pain-related symptoms in mice. Our findings also support the hypothesis that autoantibodies mediate pain-related pathophysiology in the spectrum of long COVID symptoms.

Keywords Long COVID · SARS-CoV-2 · PASC · Nervous system · IgG passive transfer · Behavioral tests

Abbreviations

CASPR2	Contactin-associated protein-like 2
COVID-19	Coronavirus-associated disease 2019
DRG	Dorsal root ganglia
EBV	Epstein-barr virus
FGS	Facial grimace scale
GFAP	Glial fibrillary acidic protein
HADS	Hospital anxiety and depression scale
Iba1	Ionized calcium-binding adapter molecule 1
IVIG	Intravenous immunoglobulin
HC	Healthy control
LC	Long COVID
MoCA	Montreal cognitive assessment
Nf-l	Neurofilament-light
NPRS	Numeric pain rating scale
PASC	Post-acute sequelae of COVID
SARS-CoV-2	Severe acute respiratory syndrome coronavirus 2
SDMT	Symbol digit modalities test

Pierre Bulpa and Charles Nicaise equally contributed as last authors

Extended author information available on the last page of the article

Published online: 29 April 2026

SGC	Satellite glial cells
UCH-L1	Ubiquitin carboxy-terminal hydrolase L1
WHO	World health organization

Introduction

Although patients with COVID-19 can recover completely, approximately 10% of SARS-CoV-2 infected people develop long-lasting symptoms after the acute phase of the disease [38]. This condition is termed as long COVID (LC) or post-acute sequelae of COVID (PASC). The US National Academies of Sciences, Engineering and Medicine defines it as "*an infection-associated chronic condition that occurs after SARS-CoV-2 infection and is present for at least 3 months as a continuous, relapsing, remitting, or progressive disease state that affects one or more organ systems*" [15]. More than two hundred symptoms have been associated with LC, such as chronic fatigue, cognitive impairment and breathing issues. It is estimated that approximately 30% of LC patients suffer from cognitive impairment (brain fog, memory loss, concentration and attention deficits, anxiety, depression) [14, 31, 45] and 30% suffer from pain-related symptoms (myalgia, arthralgia, burning or prick sensations) [5, 30, 42]. Among these symptoms, 4–8% are estimated to experience neuropathic pain, typically characterized, among others, by allodynia or hyperalgesia [30, 42]. Other studies based on self-reported assessments of neuropathic symptoms suggest a prevalence up to 25% [23, 53]. So far, the underlying pathophysiology of such LC neurologic sequelae remains elusive, and no effective treatment is available for this disabling condition of daily life.

Given the broad heterogeneity of symptoms, several mechanisms have been proposed: SARS-CoV-2 viral persistence, chronic tissue inflammation, immune dysregulation, thrombo-inflammation, or latent viruses' reactivation [43]. Among the immune dysregulation mechanisms, autoimmunity has been put forward, as it is well described as part of the post-acute infection syndrome [2]. According to large cohort retrospective studies, the risk of developing new-onset autoimmune diseases significantly increases following acute COVID-19 [8, 44, 52, 54]. Hence, we hypothesized that autoimmunity could similarly be triggered by an overstimulation of the immune system during acute SARS-CoV-2 infection and autoantibodies could arise following molecular mimicry, bystander activation or epitope spreading [19, 26, 50, 51].

COVID-19 patients with neurological manifestations carry autoantibodies targeting nervous system antigens in serum or cerebrospinal fluid (e.g. APP, BDNF, mGluR5, NMDAR, myelin proteins) [17, 34, 35, 41, 60]. Anti-G protein-coupled receptor antibodies are frequently detected in LC patients with neurological symptoms [49, 59]. Moreover, months after acute infection, autoantibodies directed against nervous epitopes (e.g. myelin, NMDAR, GAD65) can still be detected in the serum and cerebrospinal fluid of LC patients with neurological impairment [4, 16, 27, 58]. However, these findings are based on relatively limited and heterogeneous studies, and other reports have failed to identify such autoantibodies. To date, no specific autoantibody has been robustly validated or shown to be consistently present across large cohorts of LC patients. Therefore, while there is emerging evidence suggesting a possible role of autoimmunity in a subset of patients, there is currently no consensus on the presence or pathogenic relevance of autoantibodies in long COVID. Interestingly, applying therapeutic plasmapheresis to LC patients significantly improved their clinical features and was associated with a reduction of autoantibody levels [1], further supporting a potential—yet still debated—role of autoantibodies in this condition.

The aim of this study was to determine whether IgG antibodies from LC patients with neurological symptoms can bind to epitopes within the central and peripheral nervous systems and produce neuropsychiatric symptoms after passive transfer to mice. To directly implicate IgGs as the main drivers of these symptoms, the effects of purified patient IgG were compared with those of IgG-depleted serum and enzymatically-digested IgGs. We also investigated the cellular targets within the nervous system, aiming to bridge the gap between autoantibody presence and functional consequences. Following enrollment of LC patients with neurological symptoms and age- and gender-matched healthy control (HC) subjects, purified human IgGs were passively transferred into C57Bl/6J female mice. Over the two weeks post-injection, pain, cognitive, anxiety and depressive-like behaviors were followed up in those mice.

Materials and methods

Patient selection

Human ethics project was approved by the CHU-UCL Namur ethics Committee (157.2022). Written and informed consent were obtained for all study participants. For all subjects, a thorough clinical assessment was conducted by an ICU COVID expert (P.B.) and an MD general practitioner (M.J.). The relevant medical SARS-CoV-2 history (disease severity, time of infection, vaccination status) and persistent symptoms since SARS-CoV-2 infection (Table 1) as well as patients' complete medical records were reviewed. LC patients' selection relied on the 2021 WHO consensus definition. Inclusion criteria for long COVID patients (LC; $n = 13$) were: (i) 18 years of age or over; (ii) previous SARS-CoV-2 infection confirmed by a PCR or antigen test; (iii) presence of persistent symptoms (cognitive impairments,

Table 1 Patient demographics. Clinical data related to age, sex, SARS-CoV-2 infection(s), vaccination status, blood sampling and patient-reported symptoms are presented. *P* percentiles. Statistical comparisons between HC and LC groups were performed using the Mann–Whitney *U* test or Fisher's exact test, when appropriate

		HC (n=10)	LC (n=13)	*p-value*
Age (years)	Mean [range]	48 [26-61]	47.5 [28-64]	0.7435
Sex	Female Male	8 2	12 1	1.0000
Educational level	• 1 • 2 • 3	0 0 10	1 0 12	1.0000
Hospital admission during acute COVID-19	YES NO	0 10	1 12	1.0000
Date of infection with SARS-CoV-2	• March 2020 to October 2020 • November 2020 to December 2021 • January 2022 to December 2023 • Unknown	0 2 3 5	6 6 1 0	n.a.
Number of infections with SARS-CoV-2	Mean	0.89 [0-2]	1.9 [1-6]	0.0617
COVID-19 vaccination status	• Number of vaccination (mean) • Type of vaccine : - AstraZeneca - Moderna - Pfizer • Before sampling	2.44 [0-4] 2 3 6 9	3.4 [0-5] 2 2 10 12	0.0438
Time from first infection to sampling (months)	Mean [range]	27.6 [11-36]	36.2 [22-44]	0.0449
Time from last infection to sampling (months)	Mean [range]	27.6 [11-36]	21.7 [7-40]	0.2767
Patient-reported complaints at the time of sampling	• Cognitive • Depression • Pain • Fatigue	0 0 0 0	13 5 13 13	<0.0001

pain, fatigue) for at least 2 months that cannot be explained by an alternative diagnosis. Age- and sex-matched individuals without morbidities served as healthy control group (HC; $n = 10$) (Table 1). Their inclusion criteria were the same as above, except for the absence of persistent symptoms for at least 2 months since SARS-CoV-2 infection. Exclusion criteria for all participants were: (i) medical history of chronic pain, depression, cognitive impairments before SARS-CoV-2 infection; (ii) diagnosis of stroke, epilepsy, or neurodegenerative diseases (e.g. Alzheimer's disease, amyotrophic lateral sclerosis, Parkison's disease); (iii) diagnosis of autoimmune disease (e.g. rheumatoid arthritis, Sjögren's syndrome, systemic lupus erythematosus, multiple sclerosis, type I diabetes). Routine laboratory tests were systematically examined to rule out alternative diagnosis for the reported symptoms. In particular, potential infectious causes such as cytomegalovirus (CMV) and Epstein–Barr virus (EBV) infections were investigated, and thyroid dysfunction was excluded. When clinically warranted, additional autoantibody screening was performed as part of routine care to exclude common autoimmune diseases. Most patients also underwent brain imaging (CT scan, MRI, or scintigraphy) during their clinical evaluation. When neuroimaging was not performed, the neurological examination was normal and did not justify further neuroradiological investigations.

The neuropsychological assessment was performed by a trained neuropsychologist (CD) and included: Montreal Cognitive Assessment (MoCA), Symbol Digit Modalities Test (SDMT), STROOP test, D2 test, TAP Go/No go, TAP divided attention task, Beck Depression Inventory, Hospital Anxiety and Depression Scale (HADS) as well as, for pain evaluation, a Numeric Pain Rating Scale (NPRS) and DN4 questionnaire (Table 2). All the neuropsychological tests were performed on the day of blood sampling. Serum was isolated within 30 min after blood sampling and kept at 4 °C until IgG purification or was aliquoted at − 20 °C for the other protein assays.

IgG purification

For IgG purification from LC patients ($n = 13$) or HC ($n = 10$), serum was diluted 1:1 with glycine 0.1M NaCl 3M pH 8.9 and passed through a protein G column (Cytiva, Uppsala, Sweden) previously equilibrated with glycine 0.1M NaCl 3M pH 8.9. The column was rinsed with glycine 0.1M NaCl 3M pH 8.9, and the IgG-depleted sera was separately collected. The bound IgGs were eluted using glycine 0.1M pH 2.3 and immediately neutralized with Tris 1M pH 9.8. The column was then re-equilibrated with glycine 0.1M NaCl 3M pH 8.9. The eluate was dialyzed overnight at 4 °C in PBS using a 12–14 kDa dialysis membrane (Spectrum Laboratories, Rancho Dominguez, CA, USA). The concentration of IgGs was determined using a Nanodrop 1000 (Thermo Scientific, Bleiswijk, The Netherlands). Finally, the IgG solution was stored at − 20 °C.

Determination of Ig, UCH-L-1, Nf-l, and GFAP levels

Quantification of immunoglobulin isotypes (IgG, IgA, IgM) in sera and in purified IgG fractions was performed using Alinity 3 point-of-care diagnostic systems (AC01873, Abbott, Chicago, IL, USA). Quantification of IgE concentration was performed using a human IgE ELISA kit (BMS2097, ThermoFisher Scientific, Waltham, MA, USA) according to manufacturer's instructions. Neuronal and glial damage markers (Nf-l, UCH-L1, GFAP) were quantified in sera, respectively, using Quanterix SIMOA assay (Simoa® NF-light™ Advantage Kit (SR-X), Quanterix, Billerica, MA, USA) and Alinity 5 point-of-care diagnostic systems (AI01128, Abbott, Chicago, IL, USA).

Papain enzymatic cleavage

Digestion buffer (PBS, 5 mM EDTA, 20 mM cysteine-HCl, pH 7.0) was prepared extemporaneously. 2mL of immobilized papain (ThermoFisher Scientific, Waltham, MA, USA) were equilibrated by adding the digestion buffer and centrifuged at 1026 × g for 5 min to pellet the resin. This step was done twice. The IgG sample was then diluted 1:1 with the digestion buffer. Approximately 12 mL of the solution were added to the immobilized papain so that the IgG solution was adjusted to 20mg/mL. Samples were incubated overnight at 37 °C on a rotating platform. After the incubation period, the digested IgGs were separated from the immobilized papain by centrifugation (3912 × g for 5 min) to pellet the resin and collect the supernatant. The digested IgG solution was then stored at − 20 °C.

Antigen microarray

Serum samples were screened for autoantibody profiling using a commercial antigen array platform (Genecopoeia, Rockville, MD, USA). Briefly, sera were hybridized onto nitrocellulose filters adherent to glass slides and microarray slides spotted with 120 known autoantigens (PA002 OmicsArray™ Brain and Central Nervous System Disorders Antigen Microarray). Slides were incubated with fluorescently coupled anti-IgG secondary antibodies and were imaged using a GenePix 4000B scanner. The Mapix software was used to analyze raw data (Innopsys France, Carbonne, France). Raw fluorescence data were normalized to PBS controls to get the Net Signal Intensity (NSI) of each antigen in each sample. The data presented in the heatmap are NSI normalized to internal Ig control batches according to manufacturer's instructions.

Table 2 Neuropsychological assessment and biomarkers of neurodamages. Expert-based cognitive testing included measures of memory (MoCA), executive functions (STROOP, Go/No Go task), attention (SDMT, D2 test, visual and auditory attention). Anxiety (HADS), depression (HADS, Beck) and pain intensity (NPRS, DN4) were assessed based on patient-reported outcomes using standardized questionnaires. Mean values for UCH-L1, Nf-L, GFAP serum levels are expressed in pg/mL. *P* = percentiles. Statistical comparisons between HC and LC groups were performed using the Mann–Whitney *U* test or Fisher's exact test, when appropriate

		HC (n=10)	LC (n=13)	*p-value*
MoCA (points)	>26/30 **<26/30**	10 0	9 4	0.0537
STROOP Inhibition disorder (percentiles)	>P5 **<P5**	10 0	7 6	0.0461
Go/No go Inhibition disorder (percentiles)	>P2.3 **<P2.3**	10 0	7 6	0.0461
SDMT (percentiles)	>-2 **<-2**	10 0	11 2	0.4935
D2 test visual attention disorder (percentiles)	>P2.3 **<P2.3**	10 0	9 4	0.1150
Visual selective attention (percentiles)	>P2.3 **<P2.3**	10 0	9 4	0.1150
Auditory selective attention (percentiles)	>P2.3 **<P2.3**	10 0	4 9	0.0017
HADS: • **Anxiety scale** • **Depression scale**	 <8 **>8** <8 **>8**	 8 2 10 0	 3 10 4 9	 0.0274 0.0017
Beck depression inventory	<4 **>4**	9 1	3 10	0.0075
Pain intensity (NPRS/10): • **Last 4 weeks before sampling** • **On the day of sampling**	 Mean [range] Mean [range]	 0.78 [0-5] 0	 5.2 [2-9] 3.3 [0.4-8.4]	 0.0001 0.0001
DN4 (neuropathic pain)	<4 **>4**	10 0	5 8	0.0055
Serum UCH-L1 (pg/mL)	Mean [range]	60.9 [18.3-72.9]	65.6 [42.5-109.6]	0.7128
Serum Nf-l (pg/mL)	Mean [range]	9 [5.8-12.2]	7.3 [2.46-16.11]	0.5333
Serum GFAP (pg/mL)	Mean [range]	15.4 [8-25.6]	18.3 [8.48-24.96]	0.4173

Table 2 (continued)

GFAP Glial fibrillary acidic protein, *HADS* Hospital anxiety and depression scale, *MoCA* Montreal cognitive assessment, *Nf-L* Neurofilament-light, *NPRS* Numeric pain rating scale, *SDMT* Symbol digit modalities test, *UCH-L1* Ubiquitin carboxy-terminal hydrolase L1

Western blotting

Serum and purified IgG samples were mixed with 5% β-mercaptoethanol and denatured via boiling for 5 min prior to gel loading. Serum or IgG (1 µg/well) was loaded on a 10% polyacrylamide gel, separated via SDS-PAGE and transferred to a nitrocellulose blotting membrane (Protran, Amersham, Buckinghamshire, England). Membrane blocking was made using a bovine serum albumin 5% + TBS-Tween 0,1% solution for 1 h at room temperature. Membranes were incubated with a solution of 5% TBST-BSA and anti-human IgG light and heavy chains antibody (1:50 000, 109–035-044, Jackson Laboratory, Bar Harbor, ME, USA) at room temperature for 1 h. Prior to revelation, the membrane was rinsed 3 times with TBS-0.1% Tween and then incubated for 1 min in a chemiluminescent revelation solution (BM Chemiluminescence Blotting Substrate, Roche Diagnostics, Mannheim, Germany). The image acquisition was performed using an ImageQuant LAS 4000mini system (GE Healthcare, Little Chalfont, UK).

Mice handling

The experimental procedure was approved by the Animal Ethics Committee of the University of Namur (ethics project UN 23–392 and UN 24–438). Mice were housed in a temperature-controlled environment with a 12 h light/12-h dark cycle. They had access to food and water ad libitum. Behavioral experiments were performed on female C57BL/6J mice (8–10 weeks old) purchased from Charles River Laboratories (Beerse, Belgium). Mice received the human IgG solution intraperitoneally (8 mg/day) for four consecutive days. Each IgG batch isolated from one human subject was injected into a cohort of ten mice. During the two weeks post-injections, mice were submitted to behavioral tests (Fig. 1a). This experimental timeline was selected because the aim of the study was to evaluate the short-term effects of IgG transfer on mouse behavior. It was also based on previously published passive transfer studies in mice showing that pain-related phenotypes can be detected as early as 24–48 h after the first IgG injections [11, 20].

A second experimental paradigm was conducted using a modified protocol. Mice received intraperitoneally either IgG-depleted serum, papain-digested IgG, or native IgG (8mg/injection) from LC patients. Pain-related behavioral tests were performed as previously but over a period of two days (Fig. 2a). This shortened protocol was sufficient to assess pain-related behavioral responses as supported by our results from the first experimental protocol and by other studies [20]. Moreover, it enabled the detection of behavioral effects while ensuring a more efficient and appropriate use of the limited human biological material available. Mice were randomized between cages, and the experimenter (M.M.) was blinded to treatment.

Behavioral testing

Before any test, mice were moved to the experimental room in their home cages to acclimatize (10–15 min). Baseline measurements were performed before any IgG injection ('pre-IgG').

Hot and cold plates

The hot plate analgesia meter (Columbus Instruments, Columbus, OH, USA) was set to 52 °C while the cold plate system (ElectraCOOL™ TCP50™, Advanced thermoelectric, Melbourne, FL, USA) was set to 4 °C. Mice were placed onto each platform surrounded by transparent Plexiglas walls. The time the mice took to show signs of thermal distress (paw licking, jumping, hind-paw stomping) was measured. If mice did not show any of these signs, they were removed from the plate after 30 s to prevent tissue damage.

Hargreaves test

Mice were placed onto a glass surface, separated by a Plexiglass wall, and allowed to acclimate for 10 min. To observe a variation in thermal sensitivity among mice, a radiant thermal beam was placed under their left and right hind paws to provoke a withdrawal response using a Plantar Test Analgesia Meter (Model 390, IITC Life Science, Los Angeles, CA, USA). The time separating the stimulus onset and the paw withdrawal, called latency (in seconds), was recorded. If mice did not show signs of thermal distress (licking of the paw, paw withdrawal), the beam was removed after 20 s to prevent tissue damage. Each hind paw was stimulated three times in total with five minutes between each stimulation. The latencies of each individual were averaged.

Von Frey filaments

Von Frey filaments were calibrated monofilaments (0.008–2 g) used to apply a specific pressure on one animal's skin. Mice were tested in individual cages equipped with a stainless-steel wire mesh that allowed full access to the paws

(Bio-VF-M, Bioseb, Vitrolles, France). Stimulation with the filaments was limited to the medio-plantar area of the paw. One of a series of 8 Von Frey filaments, with logarithmically increasing stiffness, was applied to the plantar area for 2 to 3 s. The force applied should be sufficient to induce a slight buckling against the paw. Immediate licking of the filament stimulation area was considered a positive response to filament stimulation. The Chaplan's Up-and-Down method was used [9], meaning that the test was initiated with the 0.4 g filament and then the stimuli were presented consecutively, up or down. If there was no paw withdrawal response to the initial stimulus, a stronger stimulus was presented. If a paw withdrawal response was observed with the initial stimulus, a weaker stimulus was presented. This was done until the absence of paw withdrawal (if descending) or the presence of paw withdrawal (if ascending).

Nest building score

Mice were isolated in a new cage containing new nesting material. Seven hours post-IgG injection, nest construction was blindly evaluated by the experimenter using a rating scale from 1 to 3 (1 = no nest construction; 2 = partial nest with scattered material, 3 = perfectly constructed nest). This evaluation took place every day during the 4 days of IgG injection, and each day after the injection, the mice were isolated in a cage with new nesting material. At the end of the 4 day injection period, the mice that were initially together in the same cage were again put back together in a new cage containing a mixture of the new nest and each other's nests.

Facial grimace scale

Mice were video-recorded every day during the first week of IgG injection. They were then blindly evaluated by the experimenter and scored (0 = not present; 1 = moderately present; 2 = obviously present). Five facial expressions were analyzed: orbital tightening, nose bulge, cheek bulge, ear position, and whisker change.

Barnes maze

Briefly, the mouse was dropped in the center of an elevated circular platform (122 cm diameter) with 40 evenly spaced holes (5 cm diameter). An escape box (22,5c m length × 8,5 cm wide × 10,5 cm high) was located underneath one hole. This box was maintained at a fixed location for the whole duration of the test. Four visual cues were located at regular intervals around the table so that mice can use them to orient themselves. This test was done in three steps: *Habituation phase* (day 1)—mice were placed in the escape box for 60 s and then in the center of the table. They were allowed to explore it until they entered the escape box, or 300 s had elapsed. *Acquisition training* (day 1–5)—it started at least 1-h after the habituation phase. Three trainings each day for five days were performed during which the animals were placed in the center of the maze in a covert start box for 8 s and were then allowed to explore the maze for 180 s. If by the end the mice had not entered the escape box, they were gently guided towards the corresponding hole and allowed to remain there for 60 s. *Post-injection measures*—during the two weeks post-injection, mice only performed one trial at specific time points. Between each trial, the maze was thoroughly cleaned with ethanol to remove olfactory cues. The primary latency (time to locate the target hole) and total latency (time to enter the escape box) were recorded.

Y-maze

The Y-maze (arm's length 40 cm × 8 cm wide, center zone 8 cm diameter) was made of three symmetrical arms (A, B, C). The mouse was placed at the same end of one arm of the *Y*-shaped maze and allowed to explore it for 300 s. The total distance traveled was determined by a tracking software (EthoVision XT 18, Noldus System, Netherlands) and served as a measure of fatigue. The number of alternations between each arm (arm A, arm B, arm C) and the number of entries in each arm were monitored by a video tracking system (EthoVision XT 18, Noldus System, The Netherlands). The percentage of alternations was then calculated as follows: (total number of alternations/number of arms entered) × 100.

Elevated-plus maze

The elevated-plus maze consisted of a plus-shaped maze elevated above the ground (51 cm) with two opposite closed arms (30 cm length × 5 cm wide), two opposite open arms (30 cm length × 5 cm wide) and a central square (5 cm sides). Mice were placed at the center of the maze, head facing an open arm, and explored the maze for 300 s. The total time spent in the open and closed arms, respectively, was measured by a video tracking system (EthoVision XT 18, Noldus System, The Netherlands).

Light/dark box

The apparatus consisted of a box (50 cm length × 24 cm wide x 24cm high) equally divided into a bright and a dark compartment. An opening of 7 cm high and 7 cm wide connects the two parts. Mice were placed in the bright chamber and explored the box for 300 s. The total time spent in the dark and bright chambers, respectively, was measured by a video tracking system (EthoVision XT 18, Noldus System, The Netherlands).

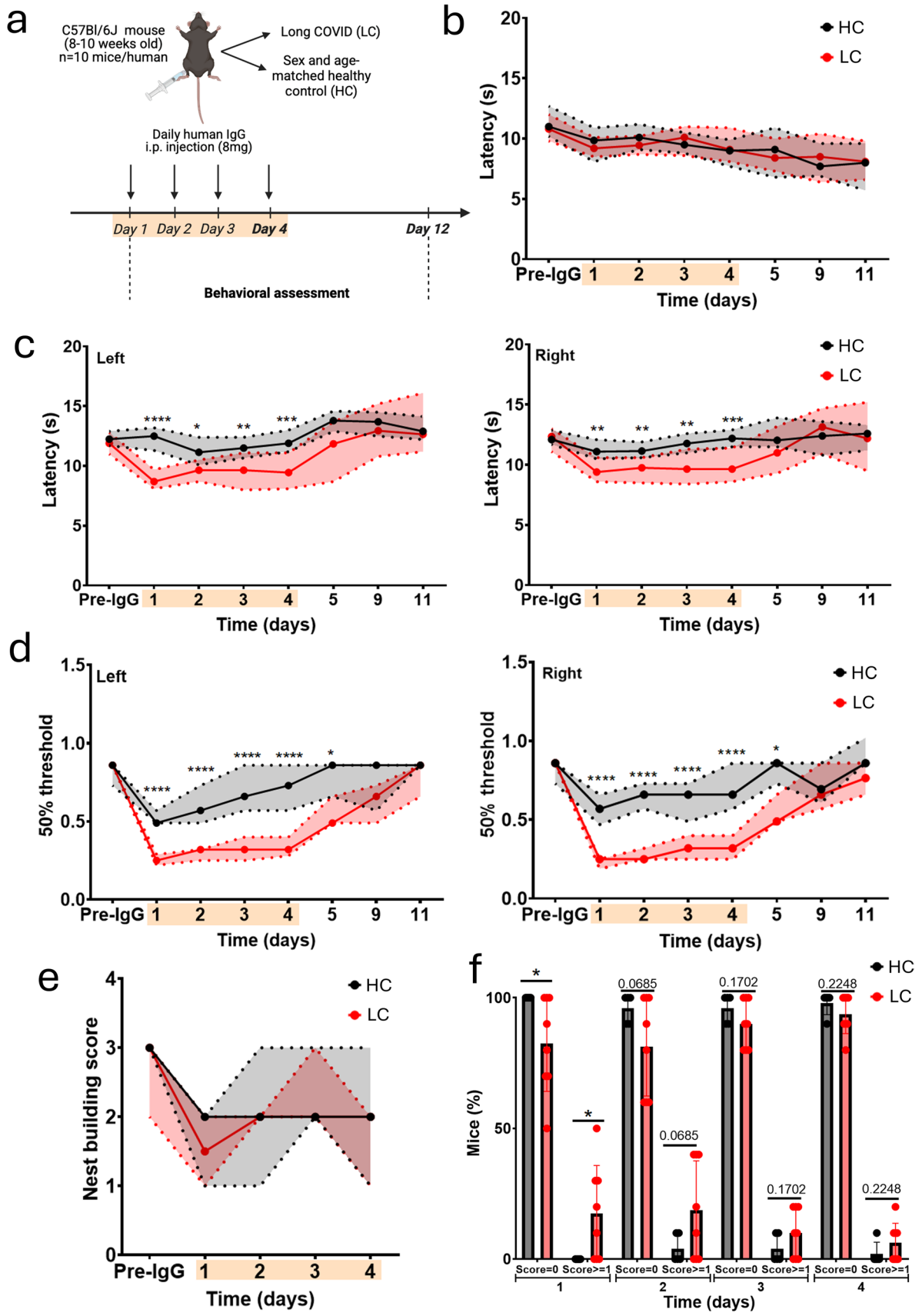
a
C57Bl/6J mouse
(8-10 weeks old)
n=10 mice/human
Long COVID (LC)
Sex and age-matched healthy control (HC)
Daily human IgG
i.p. injection (8mg)
Day 1 Day 2 Day 3 Day 4
Day 12
Behavioral assessment
b
HC
LC
Latency (s)
Pre-IgG 1 2 3 4 5 9 11
Time (days)
c
Left
Right
Latency (s)
Time (days)
d
Left
Right
50% threshold
Time (days)
e
Nest building score
Time (days)
f
Mice (%)
Score=0 Score>=1
0.0685
0.1702
0.2248
Time (days)

◂**Fig. 1** Pain-related behavioral tests in mice transferred with IgG from long COVID patients (LC) or healthy controls (HC). **a** Experimental timeline. 10 mice were used per human IgG batch. The number of human subjects included for each specific test is detailed below. The orange overlay on each timeline corresponds to the injection period. **b** Paw withdrawal latency at the hot plate test was unchanged between HC ($n=7$) and LC ($n=10$) groups. **c** Hind paw (left and right) withdrawal latency at the Hargreaves test was significantly decreased during the first four days post-injection in the LC ($n=6$) condition compared to the HC ($n=5$). **d** Hind paw (left and right) withdrawal threshold at the Von Frey filaments was significantly decreased during the first five days post-injection in the LC ($n=13$) condition compared to the HC ($n=10$). **e** The general well-being and motivation behavior were similar between groups of mice at the nest-building score ($n=5$ HC and $n=8$ LC). **f** The percentage of mice with an abnormal Facial Grimace Scale (score ≥ 1) was significantly increased on the first day post-injection in the LC group ($n=8$ LC and $n=5$ HC). Median [95% CI]. Mixed-effects model followed by a Holm-Sidak multiple comparison test between HC and LC (*$p<0.05$, **$p<0.01$, ****$p<0.0001$)

Tail suspension test

The test consisted of a tail suspension apparatus (42 cm length × 14 cm wide × 24,5cm high) allowing three mice to be tested at the time in separate compartments so that mice could not observe and interact with each other. A piece of tape was placed on the tail of the mouse, precisely 2 cm from its tip. The tape itself was attached to a hook in the middle of the suspension cage. For 360 s, the total duration of agitation and immobility of the mice suspended by their tails was recorded.

Euthanasia and histology

For euthanasia, mice were anesthetized using a Ketamine/Xylazine cocktail (120 mg/kg ketamine (Nimatek); 8 mg/kg xylazine (Sedaxylan)), perfused intra-cardially with cold 0,9% NaCl. The brain, spinal cord, and lumbar dorsal root ganglia (DRG) were freshly harvested, snap-frozen or fixed with 4% paraformaldehyde for histology analysis. Brain and spinal cord samples were dehydrated with a Leica HistoCore (Leica Biosystems, Nanterre, France) and embedded in paraffin. Ten µm-thick sections were obtained using a microtome (RM2145, Leica Biosystems, Nanterre, France). DRGs were washed with PBS and transferred to 30% sucrose solution at 4 °C for 48–72 h. Then, they were embedded in OCT compound, frozen in cold isopentane and stored at -80°C. Cryosections, 10µm in thickness, were obtained using a cryostat (CM1950, Leica Biosystems, Wetzlar, Germany).

Immunohistochemistry

Paraffin sections were dewaxed and sequentially rehydrated. Heat-induced epitope retrieval was performed using a 0.01M citrate buffer pH 6 in a 96 °C water bath for 10 min. Following endogenous peroxidase blocking with 3% hydrogen peroxide for 10 min, sections were incubated with 5% goat serum-TBS for 15 min at room temperature, and were incubated overnight at 4 °C with primary antibodies (listed in Table 3) or for 4 h at room temperature with anti-human IgG antibody diluted in 1% goat serum-TBS. Sections were then incubated with secondary antibodies (Vectastain ABC-HRP kit, Peroxidase [Mouse IgG] PK-4002 or [Rabbit IgG] PK-4001 or [Goat IgG] PK-4005, Vector Laboratories, Newark, CA, USA) for 30 min at RT. Immunolabeling was revealed using 3,3'-diaminobenzidine (DAB, K3468, Dako, Santa Clara, CA, USA). Finally, the sections were counterstained with hematoxylin and mounted with DPX medium. Observations were obtained following slide scanning using Pannoramic Flash Desk DX digital scanner (3DHistech, Budapest, Hungary).

Immunofluorescence

Mouse DRGs cryosections were washed with TBS and saturated with TBS-BSA 0.2%—Tween 0.02% for 1 h at RT. Primary antibodies (Table 3) were diluted in the saturation solution and incubated on sections at 4 °C O/N. After washing with TBS-Tween 0.02%, sections were incubated for 1 h at room temperature with secondary antibodies (Table 3). Nuclei were counterstained with Hoechst (1:200; 94,403, Sigma, St Louis, MO, USA). Sections were mounted with Mowiol and kept at 4 °C until imaging with the LSM 900 confocal microscope (Zeiss, Germany). Image analyses were performed using the software ImageJ.

Normal human DRG tissues were obtained *post-mortem* through the body donation program at the Faculty of Medicine, University of Namur (Prof. P. Garin, Laboratory of Anatomy) and were approved by the CHU-UCL Namur Ethics Committee (157.2022). Paraffin sections were dewaxed and sequentially rehydrated. Slides were washed with TBS and saturated with TBS-BSA 0.2%—Tween 0.02% for 1 h at RT. Purified IgG were diluted in the saturation solution at 25 µg/mL and incubated on section at 4 °C O/N. After washing with TBS-Tween 0.02%, sections were incubated for 1 h at RT with secondary antibody (Table 3). Nuclei were counterstained with Hoechst (1:200; 94,403, Sigma, St Louis, MO, USA). Sections were mounted with Mowiol and kept at 4 °C until imaging with Olympus BX63 epifluorescence microscope equipped with XM10 camera (Olympus Corporation, Tokyo, Japan). Image analyses were performed using ImageJ. At least 100 neuron cell bodies were analyzed per condition.

RNA extraction and quantitative PCR

Brain and DRG tissues were resuspended in 1 mL of TriZol reagent (Life Technologies, Bleiswijk, The Netherlands).

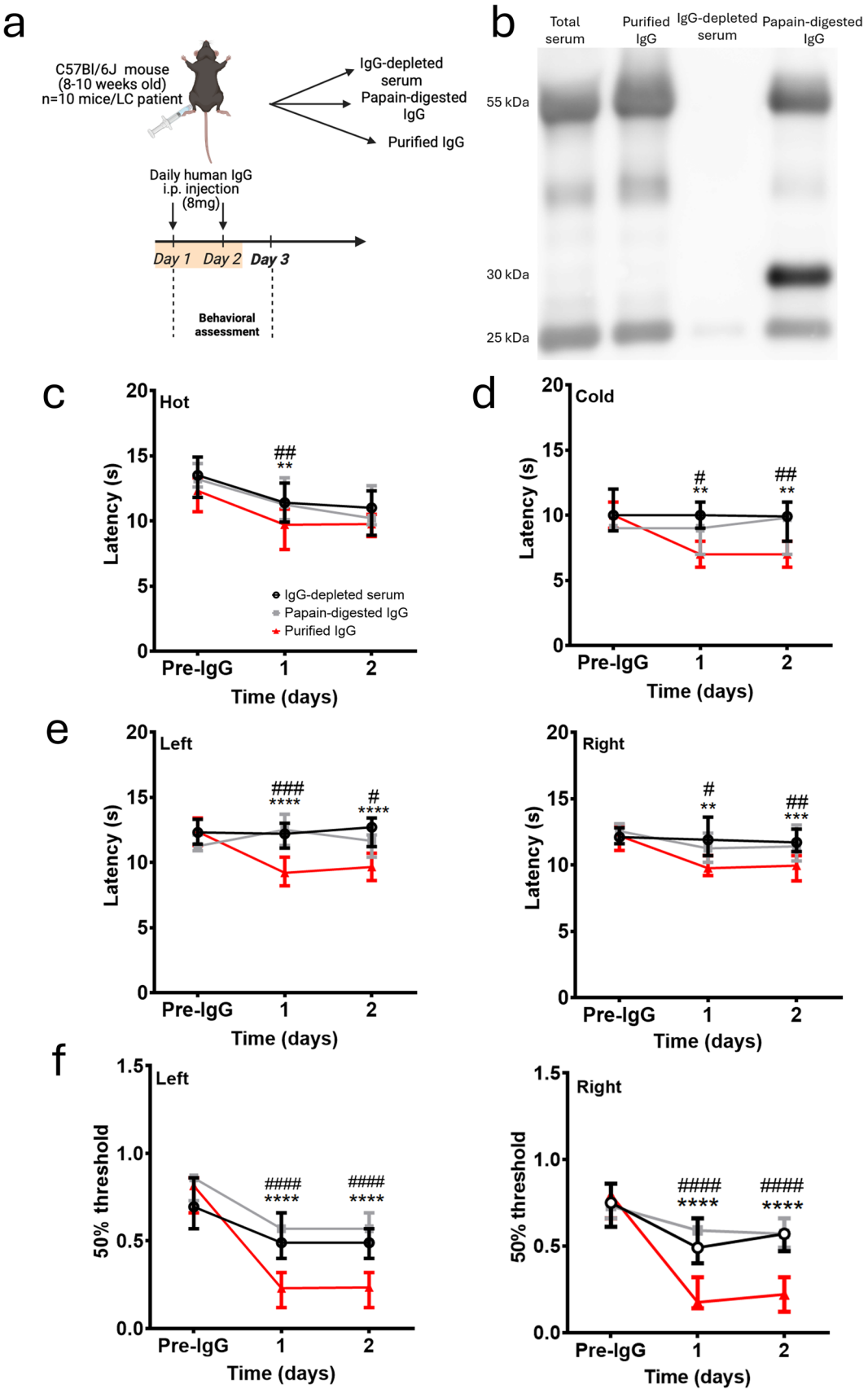
a
C57Bl/6J mouse
(8-10 weeks old)
n=10 mice/LC patient
IgG-depleted serum
Papain-digested IgG
Purified IgG
Daily human IgG
i.p. injection
(8mg)
Day 1
Day 2
Day 3
Behavioral assessment
b
Total serum
Purified IgG
IgG-depleted serum
Papain-digested IgG
55 kDa
30 kDa
25 kDa
c
Hot
Latency (s)
Time (days)
Pre-IgG
IgG-depleted serum
Papain-digested IgG
Purified IgG
d
Cold
e
Left
Right
f
Left
Right
50% threshold

◂**Fig. 2** Pain-related behavioral tests in mice transferred with purified IgG, papain-digested IgG or IgG-depleted serum, from long COVID patients. **a** Experimental timeline. 10 mice were used per patient IgG batch, $n = 3$ LC IgG batch. **b** The abundances of heavy (55 kDa), light chains (25 kDa), Fc (30 kDa) and Fab fragments (25 kDa) were assessed in total human serum, purified IgG fraction, IgG-depleted serum and papain-digested IgG fraction by immunoblotting. The presence of an extra band at 30 kDa confirmed the partial digestion of IgG heavy chains after papain incubation. **c** Paw withdrawal latency at the hot plate test was rescued the first day post-injection in mice receiving depleted serum and papain-digested IgG. **d** Paw withdrawal latency at the cold plate test was fully rescued in mice receiving depleted serum and papain-digested IgG compared to native purified IgG. **e** Hind paw (left and right) withdrawal latency at the Hargreaves test was significantly different in mice receiving depleted serum and papain-digested IgG compared to native purified IgG. **f** Hind paw (left and right) withdrawal threshold at the Von Frey filaments was fully rescued in mice receiving depleted serum and papain-digested IgG. Median [95% CI]. Mixed effects model followed by a Holm-Sidak multiple comparison test between purified IgG and the IgG-depleted serum group ($^{*}p < 0.05$, $^{***}p < 0.001$, $^{****}p < 0.0001$) and between purified IgG and the papain-digested IgG group ($^{\#}p < 0.05$, $^{\#\#}p < 0.01$, $^{\#\#\#}p < 0.001$, $^{\#\#\#\#}p < 0.0001$)

Total RNAs were isolated according to the manufacturer's instructions (High Pure RNA Tissue kit 12,033,674,001, Roche, Mannheim, Germany). RNA yield and purity were determined using a spectrophotometer NanoDrop 1000 (Thermo Scientific, Bleiswijk, The Netherlands). Total RNAs were reverse transcribed using the Super Script III Reverse Transcriptase kit according to the manufacturer's instructions (Invitrogen, Merelbeke, Belgium). cDNA samples were used to amplify genes of interest with Takyon SYBR Green kit (Eurogentec, Liège, Belgium) in a Light Cycler 96 device (Roche Diagnostics, Mannheim, Germany). Primer sequences (Eurogentec, Liège, Belgium) are as follows: *Gfap forward* 5'-GCCACCAGTAACATGCAAGA-3'; *Gfap reverse* 5'-CGGCGATAGTCGTTAGCTTC-3'; *Iba1 forward* 5'-CTTGAAGCGAATGCTGGAGAA-3'; *Iba1 reverse* 5'-GGCAGCTCGGAGATAGCTTT-3'; *Hprt forward* 5′-TGACACTGGCAAAACAATGCA-3′; *Hprt reverse* 5′-GGTCCTTTTCACCAGCAAGCT-3′. The relative gene expression was calculated using the ΔΔCq method with *hprt* as the housekeeping gene.

Statistical analysis

Data are presented as median [95% CI] or mean ± SD and the number of patients/healthy individuals included is indicated by the value of *n*. Ten mice were systematically used per patient/healthy individual IgG batch. Statistical analyses were performed on individual mouse data. Paired *t*-test (Suppl. Figure 1), Mann–Whitney U test (Figs. 4, 6b, 8b, Tables 1, 2), Welch's t-test (Fig. 8d), Fischer's exact test (Tables 1, 2), Kruskal–Wallis H test (Fig. 7b), and mixed model followed by Holm-Šídák multiple comparison test (Figs. 1b–f, 2c–f, 3a–f, Suppl. Figures 2a–e, 3a–e.) were used to determine statistical significance (set at $p < 0.05$). Statistical analyses were performed on the software GraphPad Prism (v.10.2.3, La Jolla, USA) or in the R environment (v.2025.05.1 + 513).

Results

Patients' demographics and neuropsychological assessment

A total of 25 LC patients were screened and 13 were found eligible and enrolled in this study. The reasons for non-enrollment were lack of neurologic symptoms at the time of recruitment, or pre-diagnosed autoimmune or neurologic diseases. Clinical demographics and neuropsychological test performances are presented in Table 1 and Table 2, respectively. Our LC cohort included mostly women (M:F ratio 1:12), with a mean age of 47.5 years. Average time from the first SARS-CoV-2 infection to recruitment was 36.2 ± 6.9 months. All participants of the LC cohort ($n = 13$) reported cognitive impairment, pain, and fatigue at the time of recruitment and blood sampling. Five LC patients also reported symptoms of depression, while none of the HC participants ($n = 10$) reported such complaints (Table 1). Other clinical-relevant features included the patient-reported number of infections, the dates of infection, the vaccination status or type of vaccines, and the time from last infection to sampling (Table 1).

Expert-based neuropsychological assessment revealed that 6 LC patients exhibited inhibition disorders, 4 had visual attention disorders, and 9 showed signs of auditory attention disorders. Most of these LC patients presented symptoms of depression ($n = 9$) and anxiety ($n = 10$), whereas none of the HC participants had depression and only 2 reported anxiety. All LC, but not HC, patients reported pain on the day of sampling, with an average intensity of 3.3 ± 2.84 at the Numeric Pain Rating Scale. Additionally, 8 LC patients were identified as suffering from neuropathic pain according to the DN4 questionnaire criteria. No significant differences in the serum biomarkers of neuronal or glial damage, respectively, Nf-L, UCH-L1 and GFAP, were observed between the HC and LC groups (Table 2).

IgG concentration in sera and purified fractions

IgG were purified from the serum of LC patients and HC subjects. In HC serum samples, the mean IgG concentration was 7.27 ± 1.2 mg/mL, while the IgG fraction following column G purification contained 6.74 ± 0.5 mg/mL. In LC serum samples, the mean IgG concentration was 7.30 ± 1.3 mg/mL, and 7.27 ± 1.2 mg/mL in the purified IgG fractions. These values indicate that only a minimal loss of IgG

Table 3 Primary and secondary antibodies for immunohistochemistry (IHC) or immunofluorescence (IF)

Antibody Name	Reference	Dilution	Application
cGRP	D5R8F, Cell Signaling, USA	1:200	IF
GFAP	G3893, Sigma-Aldrich, USA	1:1000	IHC
Glutamine Synthetase	Ab73593, Abcam, UK	1:100	IF
Goat anti-human IgG Alexa fluor™ 594	A11014, Life Technologies, USA	1:250	IF
Goat anti-human IgG antibody biotinylated	BA-3000-1.5, Vector laboratories, Burlingame, USA	1:50	IHC
Goat anti-Rabbit Alexa fluor™ 488	A11008, Life Technologies, USA	1:200	IF
Iba1	019-19741, FUJIFILM Wako Pure Chemical Corporation, Japan	1:1000	IHC
NeuN	D3S3I, Cell Signaling, USA	1:250	IF
NF200	286T, Cell Signaling, USA	1:400	IF
Peripherin	AB1530, Merck Millipore, Darmstadt, Germany	1:200	IF

occurred during the purification process (Suppl.Fig. 1). Other immunoglobulin isotypes (IgE, IgA, and IgM) were also quantified and showed a significant decrease following purification (Suppl.Fig. 1). This confirms that the purified fractions were specifically enriched in IgG, with minimal contamination from other isotypes.

Passive transfer of IgG from LC patients induces a transient allodynia and hyperalgesia

To investigate the potential pathogenicity of IgG from LC patients, purified IgG from LC patients or HC subjects was administered daily to C57Bl/6J mice by intraperitoneal injection (8mg/day) for four consecutive days. During the two weeks post-injections, pain-related behaviors were evaluated in mice using a battery of behavioral tests (Fig. 1a).

First, thermal sensitivity was assessed by measuring paw withdrawal latency using the hot plate and Hargreaves tests. No significant difference was observed between HC and LC groups in the hot plate test (Fig. 1b). This lack of effect in the hot plate test remained unchanged when the analysis was restricted to the subset of five LC patients who reported heat- and cold-induced pain according to the DN4 questionnaire and the Numeric Pain Rating Scale (NPRS) (Suppl. Figure 2a). On the contrary, a significant decrease in paw withdrawal latency, for both paws, was observed in the LC group in the Hargreaves test (Fig. 1c). When the analysis was restricted to patients with neuropathic pain, the thermal hypersensitivity observed in the LC group with the Hargreaves test persisted (Suppl. Figure 2b).

Second, mechanical allodynia was evaluated using the Von Frey filaments test. Passive transfer of IgG from LC patients induced a transient and significant decrease in the paw withdrawal threshold, for both paws, compared to HC (Fig. 1d). This effect was still observed when narrowing the analysis to eight LC patients who specifically experienced

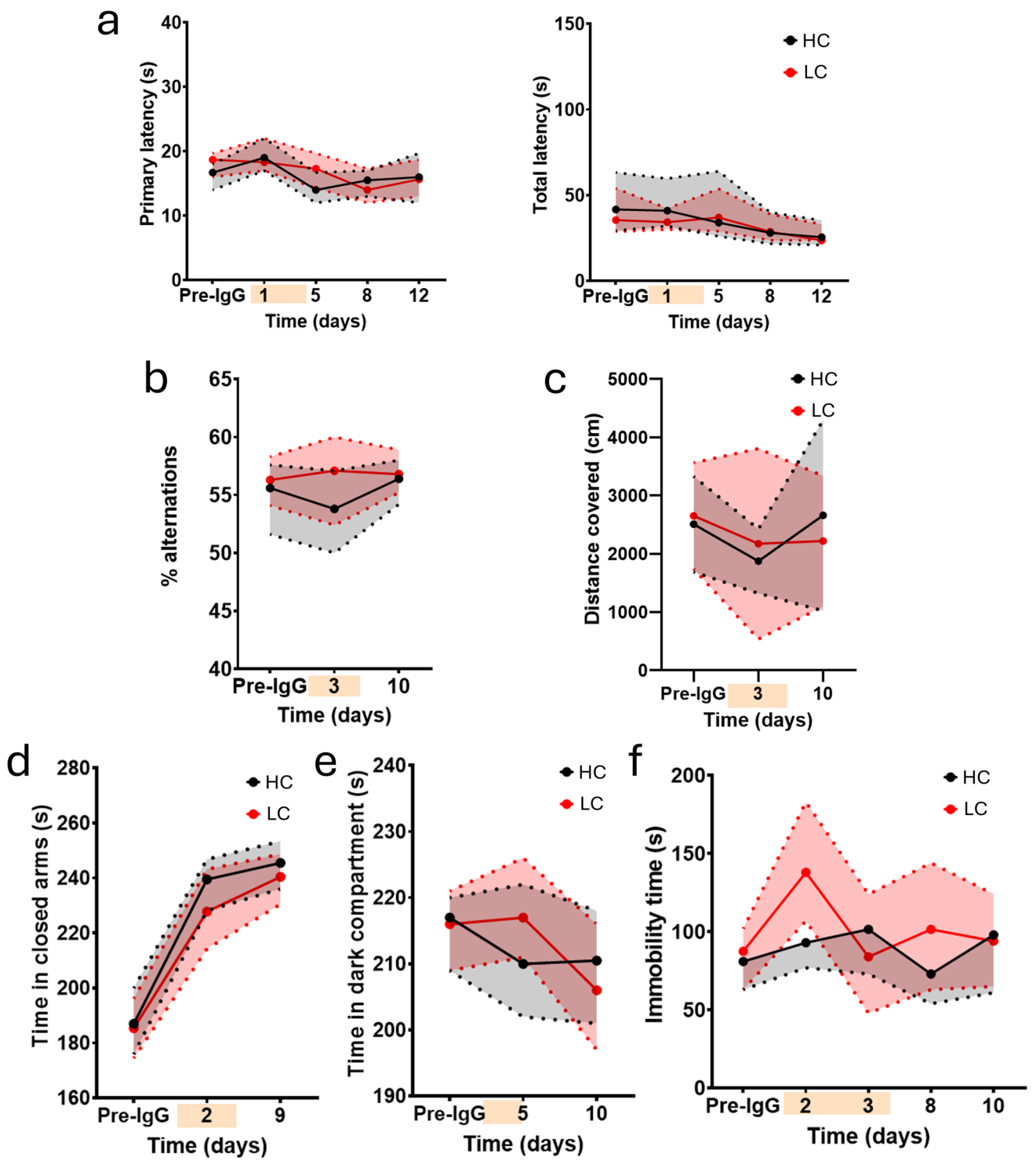

Fig. 3 Spatial memory, anxiety and depression-related behavioral tests in mice transferred with IgG from long COVID patients (LC) or healthy controls (HC). 10 mice were used per human IgG batch. The number of human subjects included for each specific test is detailed below. The orange overlay corresponds to the injection period. **a** Primary and total latencies at the Barnes maze did not differ between HC ($n=9$) and LC ($n=10$) groups. **b** Alternation between the arms of the Y-maze did not differ between HC ($n=8$) and LC ($n=10$) groups. **c** Total distance traveled in the Y-maze reflecting the general locomotor activity was unchanged between experimental conditions ($n=8$ HC and $n=10$ LC). **d** Time spent in the closed arms of the elevated-plus maze, as a measure of anxiety, was similar between groups ($n=6$ HC and $n=7$ LC). **e** Time spent in the dark compartment of the light and dark box, as a measure of anxiety, was similar between groups ($n=6$ HC and $n=7$ LC). **f** Immobility time at the tail suspension test, as a proxy of depressive-like behavior in mice, did not differ between HC ($n=6$) and LC ($n=7$) groups. Median [95% CI]. Mixed-effects model followed by a Holm-Sidak multiple-comparison test between HC and LC

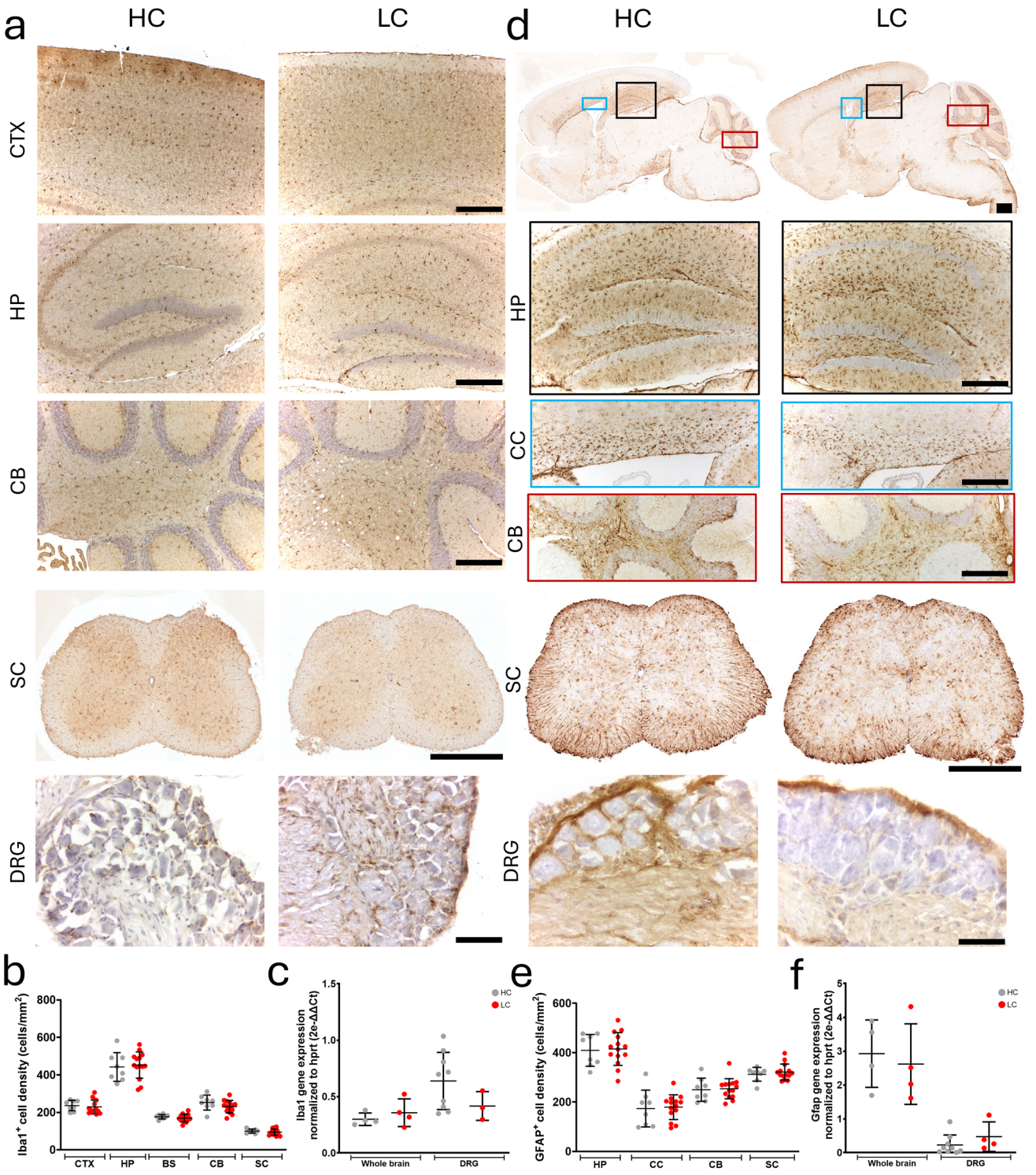

Fig. 4 Assessment of glial activation in the central and peripheral nervous systems of mice transferred with human IgG. **a** Immunolabeling of Iba1 protein in the brain, spinal cord and DRG of mice. **b** The quantification of Iba1$^+$ microglia density did not show any significant difference in the (sub)regions-of-interest between HC and LC groups. **c** The normalized expression of Iba1 mRNA did not show any significant difference in the whole-brain or DRGs between HC and LC groups. **d** GFAP protein was immunolabeled in the brain, spinal cord and DRG of mice. Scale bar represents 500 µm for brain and spinal cord and 100 µm for DRGs. **e** The quantification of GFAP$^+$ astrocyte density did not show any significant difference in the (sub)regions-of-interest between HC and LC groups. **f** The normalized expression of GFAP mRNA did not show any significant difference in the whole-brain or DRGs between HC and LC groups. Mean ± SD. Statistical analyses were computed using a Mann–Whitney U test. *p-value* = *ns*. *CTX* Cortex, *HP* Hippocampus, *BS* Brainstem, *CC* Corpus callosum, *CB* Cerebellum, *SC* Spinal cord, *DRG* Dorsal root ganglia

hypersensitivity to mechanical pressure, as reported in their DN4 questionnaire and NPRS (Suppl. Figure 2c).

Third, we assessed the general well-being of mice using the Nest-building score and the Facial Grimace Scale (FGS). No significant differences were observed in nest-building behavior between groups (Fig. 1e). However, the FGS score was significantly higher (FGS ≥ 1) in mice receiving IgG from LC patients on day 1, with no further differences detected at later time points (Fig. 1f). When we restricted the analysis to the subset of LC patients who reported mechanical hypersensitivity, similar effects were observed (Suppl.Fig. 2d–e). Abnormal FGS score was even extended until day 2 of the injection protocol (Suppl.Fig. 2e).

Pain behaviors are alleviated upon LC IgG enzymatic digestion or IgG depletion

To confirm that pain-related behaviors were mediated by IgG from LC patients, the transfer protocol was slightly adapted. In brief, IgG-depleted serum, papain-digested IgG or purified IgG fractions from the same batches of LC patients ($n = 3$) were transferred to C57Bl/6J mice for two consecutive days. Pain-related behaviors were performed during this period (Fig. 2a), as we previously demonstrated that allodynia and hyperalgesia were both triggered on the first day of transfer.

Papain is a cysteine-protease cleaving human IgG at the hinge region, leading to a fragment crystallizable (Fc) and two fragment antigen-binding (Fab) domains. A western blot validated the effective enzymatic cleavage in the papain-digested fraction, compared to the total serum, native purified IgG, and IgG-depleted serum (Fig. 2b). A band near 50 kDa, corresponding to the human IgG heavy chain, and a 25 kDa band for the light chain were detected in total and purified IgG samples. These bands were absent in IgG-depleted serum, confirming successful depletion. In the papain-digested samples, a new band at ± 30 kDa (Fc fragment) and another at ± 25 kDa (Fab fragment) were observed. However, the persistence of the 50 kDa heavy chain band indicated only partial digestion (Fig. 2b).

Thermal and mechanical hypersensitivities were abolished when mice were injected with IgG-depleted serum or papain-digested IgG, compared to those receiving native IgG from LC patients (Fig. 2c–f). While thermal hypersensitivity in the hot plate test was alleviated only on the first day under IgG-depleted serum or papain-digested conditions (Fig. 2c), the hypersensitivity to cold stimulus was abolished over the two days of the protocol (Fig. 2d).

Passive transfer of human IgG from LC patients does not trigger cognitive deficits, anxiety, or depression

We next assessed spatial working memory using the Barnes maze (long-term memory) and Y-maze (short-term memory), anxiety-related behavior using the Elevated-plus maze and Light/Dark box tests, and depressive-like behavior using the Tail Suspension Test. In the Barnes maze, no significant difference was observed between groups in either the latency to locate the target hole (primary latency) or to enter into the escape box (total latency) (Fig. 3a). Spontaneous alternation as well as total distance covered in the Y-maze did not differ between mice receiving IgG from LC patients and those receiving IgG from HC subjects (Fig. 3b, c). Similar effects were observed when the analysis was restricted to mice receiving IgG from the four LC patients with cognitive impairments (Table 2), as defined by a MoCA score below 26 (Suppl.Fig. 3a, b). In the same vein, the time spent in the closed arms of the Elevated-plus maze, in the dark compartment of the Light/Dark box, as well as the immobility time at the Tail Suspension Test were all not different in mice that received IgG from this subset of LC patients (Fig. 3d–f). Non-significant results were also obtained when the analysis was restricted to mice injected with IgG from the subset of patients with anxiety-only or depression-only outcomes (HADS score above 8) (Suppl.Fig. 3c–e).

IgG injections from LC patients do not induce microgliosis or astrogliosis

Pain-related behaviors induced in mice that received IgG from LC patients could be a consequence of neuroinflammation. Hence, we performed immunohistochemistry targeting Iba-1 to identify microglial cells and GFAP for astrocytes. We did not observe a significant difference in the density of Iba1-positive cells in different regions-of-interest of the brain or in the lumbar spinal cord (Fig. 4a, b). Similarly, there were no differences in GFAP-positive cells in the corpus callosum, hippocampus or brainstem or in the lumbar spinal cord (Fig. 4d, e). These results were further supported by RT-qPCR analyses, which showed no significant changes in *Iba1* and *Gfap* mRNA expression in either whole-brain or DRG homogenates (Fig. 4c, f).

IgG from LC patients accumulates into the peripheral nervous system but not the central nervous system

Since mice injected with IgG from LC patients exhibited increased hypersensitivity, we investigated the distribution of human IgG within the nervous system to identify potential sites of binding or action. Immunohistochemical analyses were performed on tissues collected on the 4th day of the IgG injection protocol. No immunoreactivity for human IgG was found in the brain parenchyma and spinal cord (Fig. 5a, b), except in the connective tissue and blood vessels located in the choroid plexuses and meninges of injected mice, in both transferred groups (Fig. 5a).

Respective tissues from naive mice, which did not undergo any transfer of human IgG, were devoid of immunoreactivity, and served as controls for antibody species specificity. In contrast, human IgG were detected in the ganglionic cell body-rich area, mainly in the peri-neuronal spaces of dorsal root ganglia (DRG) of the HC group (blue arrowheads), while in the LC group, immunolabeling onto neuron cell bodies was observed (black arrows, Fig. 5c),

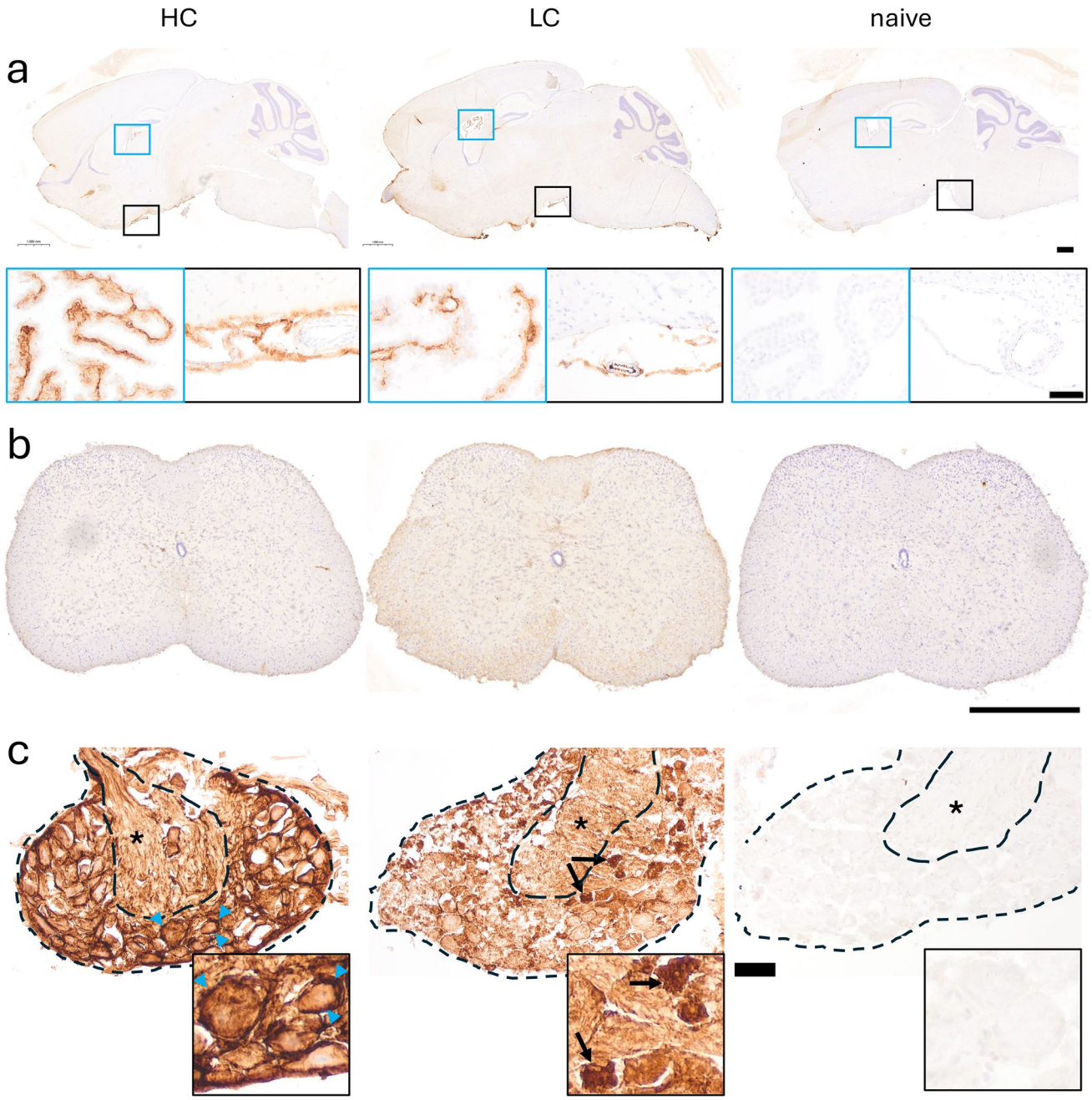

Fig. 5 Distribution of transferred human IgG throughout the central and peripheral nervous systems of mice. **a** In brains, human IgG immunoreactivity was visualized in the connective tissue of choroid plexuses (blue square) and in the meningeal layer (black square), while it was not detected in the parenchyma for both HC and LC conditions. No immunoreactivity was seen in the brains of naïve mice that were not transferred with human IgG. Scale bar represents 500 µm. Inset scale bar represents 50 µm. **b** In lumbar spinal cords, no immunoreactivity was observed in both HC and LC conditions, as well as in naïve mice. Scale bar equals 500 µm. **c** In lumbar DRG, human IgG immunoreactivity was observed in the fiber-rich area (black star) and in the peri-neuronal spaces (blue arrowheads) in the HC condition. Distribution of human IgG was strikingly different in the LC condition, with immunoreactivity on the sensory neuron cell bodies (dark arrows). No immunoreactivity was seen in the DRG of naïve mice. Scale bar represents 50 µm

indicating a differential accumulation of IgG in peripheral sensory structures.

IgG from LC patients binds to sensory neurons in the lumbar dorsal root ganglia

To identify the cell types targeted by human IgG in the DRG, we performed double immunofluorescence against neuron cell bodies (NeuN) and satellite glial cells (Glutamine Synthetase). As for immunohistochemistry, human IgG from HC subjects were detected in the peri-neuronal network of the DRG. Human IgG from LC patients colocalized with NeuN, but not with glutamine synthetase (Fig. 6a, c). The percentage of NeuN + /IgG + cells was significantly higher in DRG from mice injected with LC patient IgG than in DRG transferred with HC IgG (Fig. 6b). When characterizing DRG neuron subtypes using fiber-specific markers, we observed that approximately 40% of $NF200^+$ neurons (Aβ and Aδ fibers) colocalized with human IgG, whereas about 18% of $peripherin^+$ neurons (C-fibers) and 12% of $cGRP^+$ neurons (C-fibers and Aδ fibers) showed IgG colocalization (Suppl.Fig. 4a, b). The colocalization between human IgG and sensory neurons was no longer observed when mice received IgG-depleted serum or papain-digested IgG compared to mice receiving purified LC IgG (Fig. 7a, b).

Targeted antigen screening failed to identify a common autoreactivity profile across LC sera

When applied onto human *post-mortem* DRG tissue, IgG batches showed a differential affinity between those from HC individuals and LC patients. While IgG from both groups bound to satellite glial cells (yellow arrowheads), IgG from LC patients specifically localized to sensory neuron soma, appearing as a punctiform immunoreactivity (white arrows) (Fig. 8a). The quantification of puncta per cell revealed a highly significant increase in the DRG slices exposed to LC IgG, compared to HC IgG (Fig. 8b).

We next sought to identify the putative antigens differentially recognized by IgG (auto)antibodies in LC patients. Serum samples were screened against a panel of 120 known neurological disease-associated autoantigens (Fig. 8c). No striking difference was observed between the autoreactivity profiles of LC and HC groups, due to a high degree of inter-individual heterogeneity and the limited number of patient samples. Among the candidate autoantibodies close to the significance threshold, anti-HSPA5/GRP78 levels ($p = 0.064$) were found to be nearly doubled in the serum of LC patients, while NOVA1 and RBPJ antibodies ($p = 0.057$ and $p = 0.049$, respectively) tend to be downregulated (Fig. 8d).

Discussion

Although the underlying mechanisms behind long COVID remain unclear, growing evidence points towards a post-viral autoimmune syndrome, besides other concomitant drivers such as viral persistence. In this study, we specifically investigated the pathogenic effect of post-COVID circulating IgG and sought to identify their cellular targets within the nervous system. One approach to directly assess the causality is to perform passive transfer of purified human IgG to mice. When mice received IgG from LC patients, they exhibited increased mechanical and thermal sensitivity which resolved after cessation of IgG injections. This study strengthens (non-peer reviewed yet) data obtained on independent long COVID cohorts (USA and NL) [10, 48]. Several studies have shown that passive transfer of IgG from patients (fibromyalgia, complex regional pain syndrome) can recapitulate the pain symptomatology in mice [3, 20, 22]. Interaction between the nervous and immune systems in the context of autoimmune diseases has been increasingly investigated in the pathophysiology of chronic pain conditions and is nowadays referred to as 'autoimmune pain'. For instance, passive transfer of contactin-associated protein-like 2 (CASPR2) antibodies from neuropathic patients has been shown to trigger mechanical allodynia in mice [13]. Growing attention is also being paid to autoimmune diseases following viral infection. For instance, cases of rheumatoid arthritis are described following Epstein-Barr virus (EBV) infection [40]. A breakdown of self-tolerance and molecular mimicry are thought to play a central role, as anti-citrullinated protein antibodies (ACPA) directed against the EBV nuclear antigen-1 (EBNA-1) can cross-react with citrullinated fibrinogen in inflamed synovial tissue [25, 36].

In the context of long COVID pain-related symptoms, the exact antigenic target(s) still need to be identified, knowing that a plethora of autoantibodies targeting nervous system epitopes have already been detected in the serum of patients [4, 16, 27, 49, 58, 59]. Functional investigations of these autoantibodies still need to determine whether they are pathogenic or accessory antibodies devoid of clinical significance. Some research outcomes demonstrated that LC patients have functional anti-GPCR antibodies (anti-β_2 adrenoceptor, muscarinic M2 receptor, α_1 -adrenoceptor, endothelin receptor, nociceptin receptor) [24, 59]. Moreover, the serum concentration of these autoantibodies is correlated to disease severity [6, 27, 49]. Interestingly, the combination of β_2 adrenoceptor and muscarinic M2 receptor antibodies was previously identified in patients with complex regional pain syndrome [29]. Most autoantibodies described in LC patients have been reported to target extracellular antigens. However,

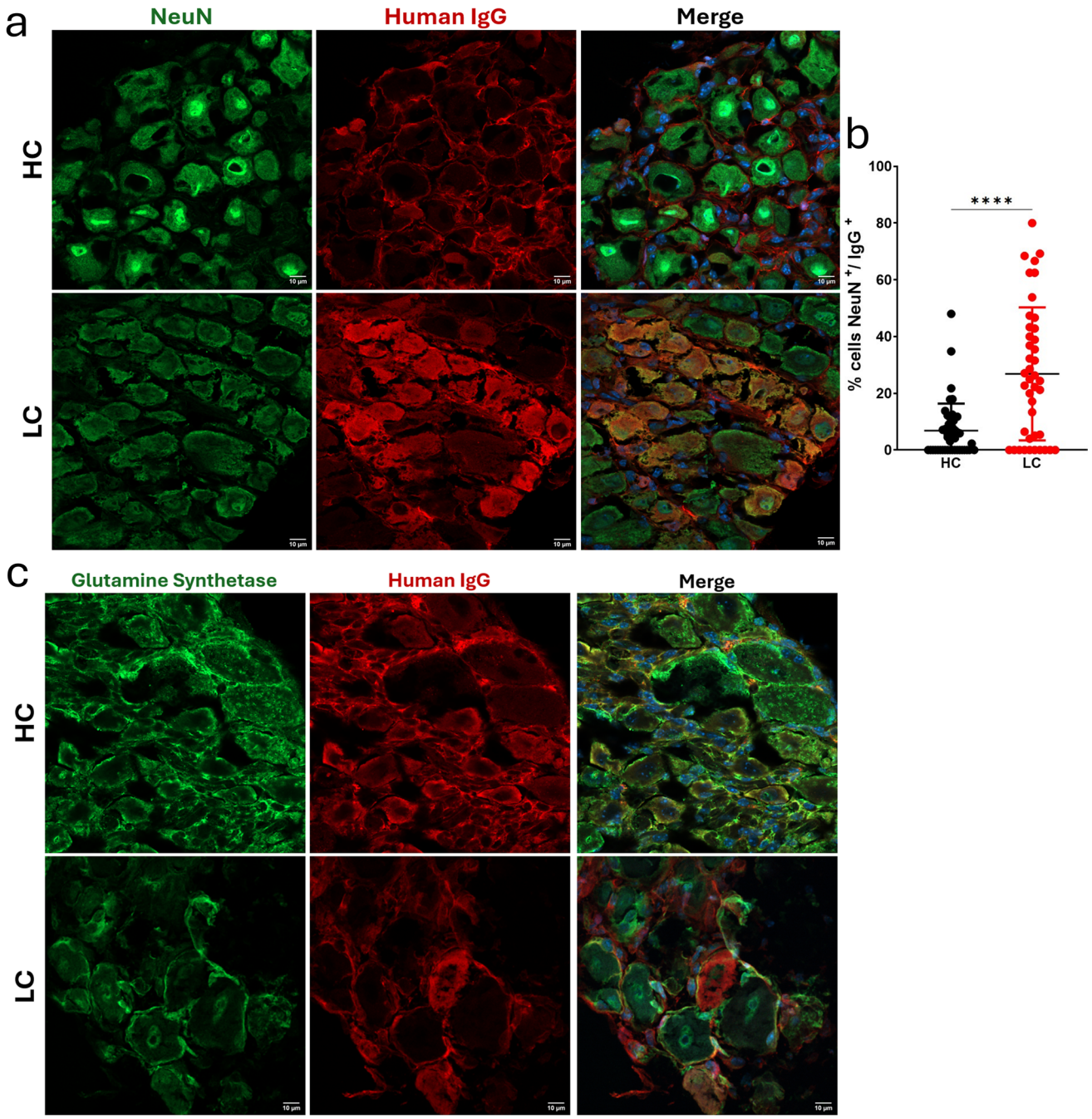

Fig. 6 Tissue distribution of IgG from long COVID patients (LC) or healthy controls (HC) in the mouse DRGs. Human IgG were immunolabeled using fluorescent anti-human IgG antibody (red). Nuclei were counterstained with Hoechst (blue). **a** Neuronal nuclei and cell bodies in the murine DRG were co-labeled using fluorescent anti-NeuN antibody (green). **b** Quantification of $NeuN^+/IgG^+$ cells was performed using FIJI ImageJ and revealed a significant increase in double immunolabeled cells in the LC condition compared to the HC group. Each dot represents a colocalization. DRGs included in the analysis were representative from 4 HC conditions ($n=8$ mice) and 3 LC conditions ($n=5$ mice). Mean ± SD. Statistical analyses were performed using a Mann–Whitney *U* test (****$p<0.0001$). **c** Satellite glial cells were immunostained using fluorescent anti-glutamine synthetase antibody (green). No colocalization with human IgG was ever evidenced with glutamine synthetase. Scale bar represents 10 µm

our immunofluorescence experiments revealed a predominantly intracellular staining pattern within the soma of sensory neurons. This observation may be explained by emerging evidence of autoantibodies directed against intracellular neuronal targets identified in both serum and cerebrospinal fluid of patients with post-COVID

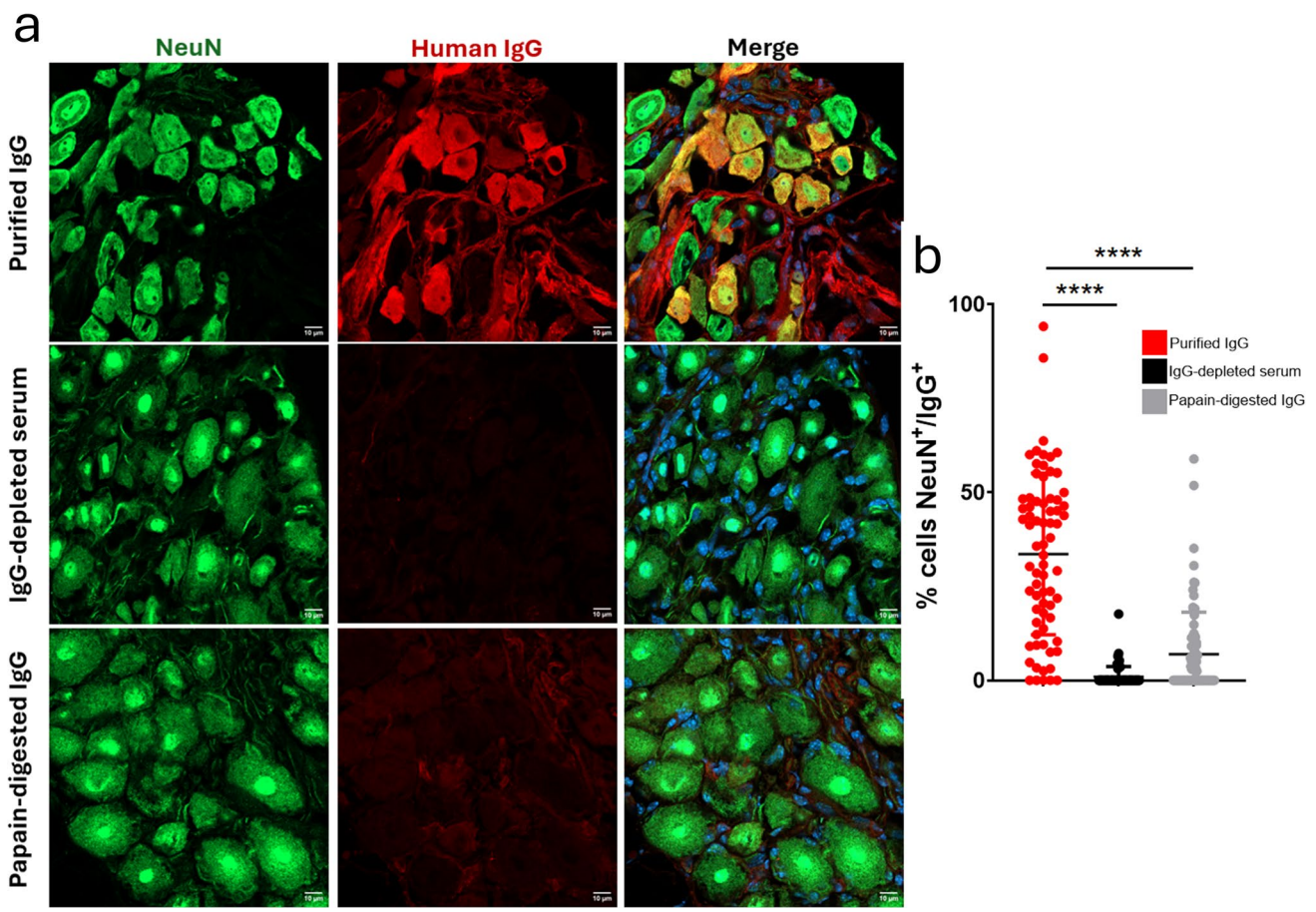

Fig. 7 Detection of human IgG in the mouse DRG after transfer of native IgG, depleted serum, or papain-digested IgG from long COVID patients. Human IgG were immunolabeled using fluorescent anti-human IgG antibody (red). Nuclei were counterstained with Hoechst (blue). **a** Neuronal nuclei and cell bodies in the murine DRG were co-labeled using fluorescent anti-NeuN antibody (green). **b** Quantification of $NeuN^+/IgG^+$ cells was performed using FIJI ImageJ. The transfer of IgG-depleted serum or papain-digested IgG significantly abolishes their detection in the mouse DRG. Each dot represents a colocalization. DRG included in the quantitative analysis were from matched LC IgG-depleted serum ($n=12$ mice), papain-digested IgG ($n=13$ mice), and purified IgG ($n=10$ mice). Mean ± SD. Statistical analyses were performed using a Kruskal–Wallis comparison test (****$p<0.0001$). Scale bar represents 10 µm

neurological syndromes, including anti-GAD (glutamate decarboxylase) and anti-ELAVL2 (neuronal nuclear antigen) antibodies [46, 57]. In addition, anti-FGFR3 autoantibodies, which have been implicated in small fiber neuropathy, have also been described in LC patients [37]. These antibodies recognize epitopes spanning both extracellular and intracellular domains of the receptor [7, 47, 55]. Furthermore, recent high-throughput screening approaches in Long COVID cohorts have identified persistent autoantibodies directed against a broad range of intracellular neuronal antigens, some of which have been associated with neurocognitive symptoms [48]. Taken together, these findings support the potential clinical relevance of the intracellular staining pattern observed in our study. Nevertheless, further investigations will be required to identify the antigenic targets of these autoantibodies and determine whether they consistently recognize defined intracellular epitopes in Long COVID patients.

Our findings further support the involvement of IgG in the symptomatology of LC patients, as well as their structural integrity as demonstrated by the alleviation of pain phenotype when mice were transferred with papain-digested IgG. The same relief effect was observed when mice received IgG-depleted serum, which mimics, from a translational point-of-view, immunoglobulin apheresis. Clinical improvement has been reported following therapeutic apheresis [1] or treatment with intravenous immunoglobulin (IVIG) [39, 56]. As such, IVIG can neutralize autoantibodies, saturate neonatal fragment crystallizable receptors (FcRNs) and inhibit subsequent complement activation [39]. Ongoing clinical trials (NCT05350774; NCT06305793; NCT06524739) are evaluating IVIG efficacy on LC patients.

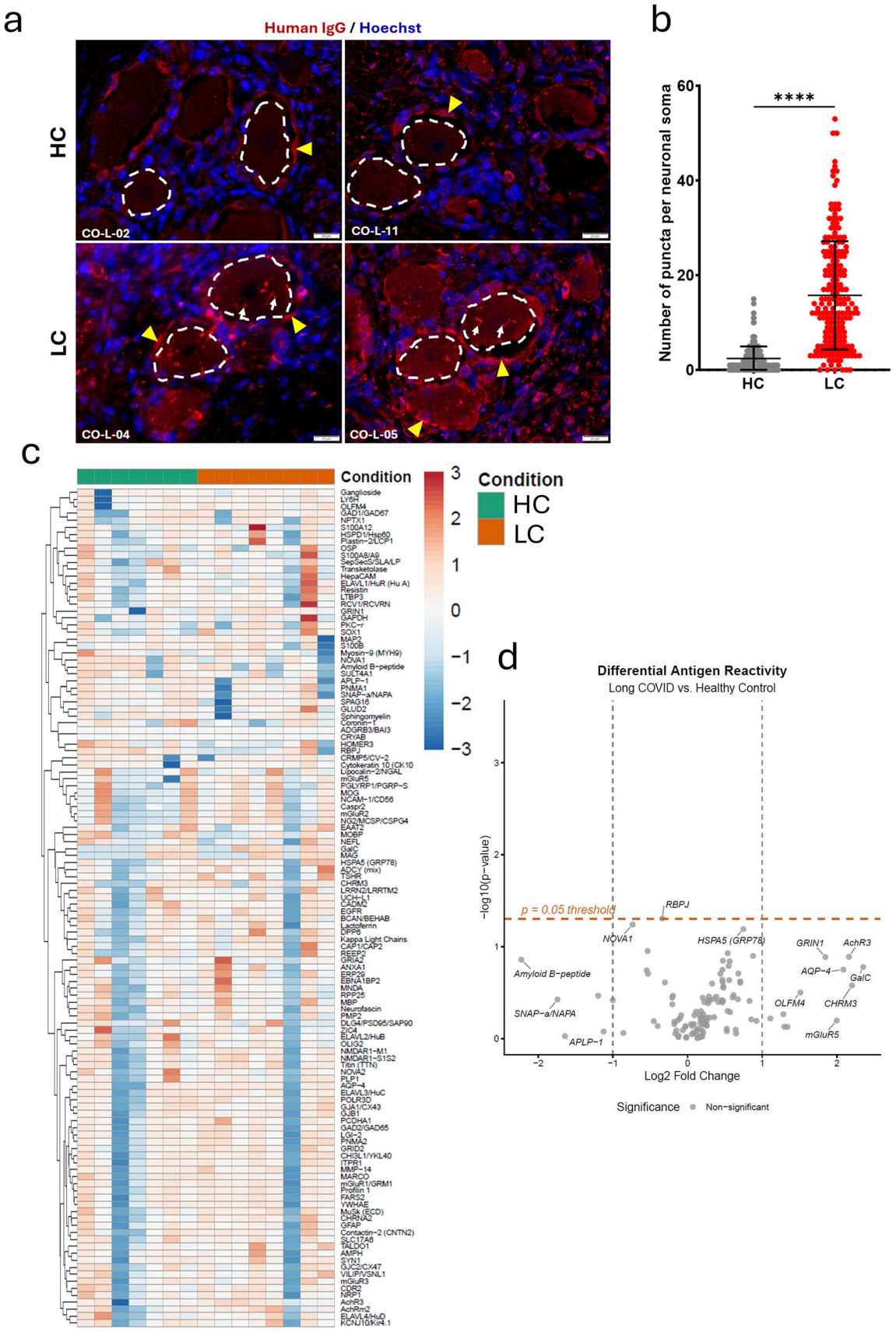
a
Human IgG / Hoechst
HC
LC
CO-L-02
CO-L-11
CO-L-04
CO-L-05
b
Number of puncta per neuronal soma
****
HC
LC
c
Condition
HC
LC
d
Differential Antigen Reactivity
Long COVID vs. Healthy Control
p = 0.05 threshold
RBPJ
NOVA1
HSPA5 (GRP78)
GRIN1
AchR3
AQP−4
GalC
OLFM4
CHRM3
mGluR5
Amyloid B−peptide
SNAP−a/NAPA
APLP−1
−log10(p−value)
Log2 Fold Change
Significance
Non−significant

◂**Fig. 8** Binding of IgG from long COVID patients (LC) or healthy controls (HC) towards human DRG tissue and levels of autoantibodies associated with known neurological disorders. **a** Human IgGs were incubated onto normal *post-mortem* DRG tissue, then detected using fluorescent anti-human IgG antibody (red). Nuclei were counterstained with Hoechst (blue). IgG from LC patients displayed a distinct localization (white arrows) compared with IgG from HC individuals. While IgG from both groups bound to satellite glial cells (yellow arrowheads), IgG from LC patients specifically localized to sensory neuron soma, appearing as punctate immunoreactivity (white arrows). **b** Quantification of puncta per neuronal soma using FIJI ImageJ revealed a significant increase in punctate IgG immunoreactivity in the LC group compared to controls. Purified IgG included in the analysis were from independent HC and LC samples ($n=4$). Mean ± SD. Statistical analyses were performed using a Mann–Whitney *U* test (****$p<0.0001$). Scale bar represents 20 µm. **c** Heatmap displaying the antibody reactivity profile for 120 analyzed antigens in HC ($n=7$) and LC ($n=8$) patients. The color of each cell represents the row-wise Z-score, indicating the number of standard deviations a patient's reactivity is from the mean of all patients for that specific antigen. Antigens are organized by hierarchical clustering to group those with similar profiles. **d** Volcano plot showing on the *x*-axis the log Fold Change and on the *y*-axis the log of the *p*-value. Statistical comparisons were performed using a Welch's *t*-test

Thompson and others reported that on nine LC patients included with immune dysregulation, six were treated with IVIG for three months and they experienced both symptomatic and laboratory improvements along with the ability to return to work [56]. Similarly, sixteen LC patients with small fiber neuropathy symptoms, of whom nine were treated with IVIG 17 months post-acute infection. At six months post-treatment, all patients showed symptoms improvement, with six presenting complete resolution and three with substantial improvement of neuropathic symptoms [37]. Altogether, these observations strongly suggest that treatments targeting autoantibodies can alleviate pain-related symptoms.

Brain fog, attention, and concentration deficits accounting among the most prevalent symptoms in LC patients, we investigated whether passive transfer of IgG mimicked cognitive impairments in mice. Our results showed that mice did not experience memory impairment, anxiety-like or depressive-like behaviors, or fatigue. Immunohistochemistry against human IgG failed to detect IgG in memory- or cognition-associated brain regions (hippocampus and cortex). Finally, no signs of brain inflammation were observed in mice that received an injection of IgG from patients with long COVID. Thus, either IgGs do not play a role in the cognitive impairment of long COVID patients or our mouse model cannot fully recapitulate human pathology. For example, human IgG might not recognize murine epitopes or might not cross an intact blood–brain barrier.

Unlike brain or spinal cord parenchyma, transferred human IgG were found in murine lumbar dorsal root ganglia (DRG) with distinct patterns: in the peri-neuronal spaces in the HC group and on neuronal cell bodies in the LC group. The peri-neuronal distribution observed in controls is not unexpected, as DRG are highly vascularized structures endowed with fenestrated capillaries that allow permeability to both low and high molecular weight molecules [28]. IgG from LC patients colocalized with neuron cell bodies but not with satellite glial cells (SGC) in mouse DRGs, and with both neuron soma and SGCs when they were applied ex vivo onto human DRGs. Notably, the mechanism underlying the punctate pattern of immunoreactivity observed with patient IgG on human DRG neurons remains unclear, although it may be consistent with the clustering of neuronal membrane proteins, including ion channels or receptors. The findings differ from other preprints reporting IgG binding to murine DRG with no group differences [10, 48]. In contrast, IgG from fibromyalgia patients primarily target SGC [3, 20] while in small fiber neuropathy, anti-plexin D1 antibodies specifically bind to nociceptive neurons [18]. Passive transfer of these antibodies to mice induced mechanical and thermal sensitivity [3, 18, 20]. More specifically in our study, IgG from LC patients preferentially targeted subsets of mouse sensory neurons, particularly A-fibers and, to a lesser extent, C-fibers. A-fibers can be divided into two main categories: Aβ-fibers, which are involved in proprioception and Aδ-fibers which mediate mechanoreception and nociception. C-fibers participate in nociception and thermoception. This dual involvement in both A and C-fiber populations has already been reported in the context of small fiber neuropathy [12]. The pronociceptive effects of IgG from LC patients may involve immune complexes interacting with Fc gamma receptors (FcγR) expressed by sensory neurons. Such interaction can modulate nociceptive signaling by modulating neuronal excitability [32]. Consistently, mechanical allodynia and DRG hyperexcitability were no longer present in nerve-injured FcγR-deficient mice [33]. Although binding of IgG-immune complexes to FcγR may have promoted inflammation [32], neither astrocytic nor microglial activation was evidenced in DRG tissues, brain and spinal cord in our model of passive transfer.

A major challenge in LC research is differentiating newly developed post-infectious symptoms from pre-existing, subclinical, or previously undiagnosed conditions that only became apparent after infection. The present study bears limitations, the first one being the limited number of LC patients and the overrepresentation of female individuals in the cohort compared to overall LC prevalence. However, the patients were carefully selected to ensure a high degree of homogeneity, thus strengthening the observed results. Second, although passive transfer models are valuable tools to demonstrate the pathogenic potential of antibodies, they typically rely on short-term, repeated high-dose administrations of IgG. As such, they may not fully reproduce the prolonged and complex immune interactions occurring in patients with a chronic condition. In this paradigm, it should be kept in mind that human IgG may not—fully or at all—recognize

murine epitopes or efficiently bind to the murine Fc receptor that could mediate downstream pathogenic events. In addition, patient heterogeneity, particularly regarding their clinical manifestations, suggests that only certain autoantibodies are present in subsets of patients and capable of inducing symptoms in mice, while others have no effect. Also, our study only used female mice as LC patients are mainly women, and it is well-known that pain and autoimmune mechanisms may involve sex-specific pathways that may not be fully recapitulated in male mice [21]. Finally, our antigen microarray failed to identify differentially expressed autoantibodies, because it used a biased approach toward 120 known nervous system-derived autoantigens and thus may have missed relevant genuine targets. Moreover, the immobilization process of the antigens on the array may alter the native structure of complex proteins, such as ion channels or receptors. As a result, conformational epitopes may be partially lost or inaccessible. Therefore, negative signals on this antigen array do not exclude the presence of autoantibodies recognizing conformational or structurally dependent epitopes, which would require complementary approaches, such as ELISA or cell-based assays, to be detected. Interestingly, data from a preprint, based on the screening of more than 21,000 human antigens, suggest unusually high levels of autoantibodies targeting the MED20 and USP5 proteins in the serum of LC patients; however, no specific causal relationship with the disease phenotype has yet been demonstrated [48]. Although evidence suggests differential binding of patient-derived IgG to human DRG neurons, further studies are needed to identify the specific autoantibody(ies), using unbiased autoantibodyome screening, as well as to elucidate their mechanisms-of-action on DRG structures or related nerve endings. In that vein, complementary experiments using in vitro approaches, based i.e. on human iPS-derived sensory neurons, might focus on a potential antibody-dependent cellular cytotoxicity or a modulation of their intrinsic excitability.

Conclusion

In conclusion, our data comfort the hypothesis of autoimmunity underlying pain-related symptoms in LC patients while providing new insights on the targets of these IgG, which are sensory neurons of lumbar dorsal root ganglia (DRG). Future research should focus on investigating the antigenic target and mechanisms behind DRG sensory neurons dysfunction.

Supplementary Information The online version contains supplementary material available at https://doi.org/10.1007/s00401-026-03019-0.

Acknowledgements Margaux Mignolet is supported by an FNRS/FRIA doctoral fellowship. This research program benefited from funding granted to Charles Nicaise (FNRS CDR J.0147.22). We thank Dr. Dominique Butenda Babapu (CHU-UCL Namur) for referring LC patients and Dr. Caroline Meyer (CHU-UCL Namur) for providing the pain-related questionnaires. We acknowledge Dr. Benoît Vokaer who instilled the seminal idea of IgG-mediated pain symptoms. We also thank Mrs. Florine Barthélémy for her technical help and all staff members from the Laboratory of Anatomy (Université de Namur). This research was made possible thanks to access to the microscope facility of the "Plateforme Technologique Morphologie – Imagerie" and the "Plateforme Technologique Sciences de la Vie" (Université de Namur). We would like to thank all the participants in the study for their contribution.

Author contributions Conceptualization: C.N., N.G., P.B., M.M.; Methodology M.M., V.B., K.D.S, T.F.; software, M.M., T.F.; validation, M.M., C.N.; formal analysis M.M., T.F.; investigation M.M., T.F.; resources V.B., K.D.S., C.D., F.G., M.J., P.B., P.G.; data curation M.M., T.F.; writing—original draft preparation M.M., C.N.; writing-review and editing M.M., N.G., J.G., P.B., C.N.; visualization M.M., C.N.; supervision C.N., N.G., P.B.; projection administration C.N.; funding acquisition C.N.

Funding Fonds De La Recherche Scientifique—FNRS.

Declarations

Conflict of interest The authors declare no competing interests.

References

1. Achleitner M, Steenblock C, Dänhardt J, Jarzebska N, Kardashi R, Kanczkowski W et al (2023) Clinical improvement of Long-COVID is associated with reduction in autoantibodies, lipids, and inflammation following therapeutic apheresis. Mol Psychiatry 28:2872–2877. https://doi.org/10.1038/s41380-023-02084-1
2. Altmann DM, Whettlock EM, Liu S, Arachchillage DJ, Boyton RJ (2023) The immunology of long COVID. Nat Rev Immunol 23:618–634. https://doi.org/10.1038/s41577-023-00904-7
3. Berwick RJ, Sahbaie P, Kenny G, Guo TZ, Neiland H, Andersson DA et al (2025) Postacute COVID-19 syndrome and fibromyalgia syndrome are associated with anti-satellite glial cell IgG serum autoantibodies but only fibromyalgia syndrome serum-IgG is pronociceptive. Pain 166:397–408. https://doi.org/10.1097/j.pain.0000000000003629
4. Boesl F, Goereci Y, Gerhard A, Bremer B, Raeder V, Schweitzer F et al (2024) Cerebrospinal fluid findings in patients with

neurological manifestations in post-COVID-19 syndrome. J Neurol 271:59–70. https://doi.org/10.1007/s00415-023-12092-4
5. Calvache-Mateo A, López-López L, Martín-Núñez J, Heredia-Ciuró A, Granados-Santiago M, Ortiz-Rubio A et al (2023) Pain and clinical presentation: a cross-sectional study of patients with new-onset chronic pain in Long-COVID-19 syndrome. Int J Environ Res Public Health 20:4049. https://doi.org/10.3390/ijerph20054049
6. Ceccarini MR, Bonetti G, Medori MC, Dhuli K, Tezzele S, Micheletti C et al (2023) Autoantibodies in patients with post-COVID syndrome: a possible link with severity? Eur Rev Med Pharmacol Sci 27:48–56. https://doi.org/10.26355/eurrev_202312_34689
7. Chamessian A, Tavares-Ferriera D, Payne M, Govindarajan R, Pestronk A, Bertels Z et al (2025) Expression of fibroblast growth factor receptor 3 (FGFR3) in the Human Peripheral Nervous System: implications for the putative pathogenic role of FGFR3 autoantibodies in neuropathy. bioRxiv. https://doi.org/10.1101/2025.03.03.639509
8. Chang R, Yen-Ting Chen T, Wang SI, Hung YM, Chen HY, Wei CJ (2023) Risk of autoimmune diseases in patients with COVID-19: a retrospective cohort study. EClinicalMedicine 56:101783. https://doi.org/10.1016/j.eclinm.2022.101783
9. Chaplan SR, Bach FW, Pogrel JW, Chung JM, Yaksh TL (1994) Quantitative assessment of tactile allodynia in the rat paw. J Neurosci Methods 53:55–63. https://doi.org/10.1016/0165-0270(94)90144-9
10. Chen H-J, Appelman B, Willemen H, Bos A, Prado J, Geyer CE et al (2024) Transfer of IgG from Long COVID patients induces symptomology in mice. bioRxiv. https://doi.org/10.1101/2024.05.30.596590
11. Cuhadar U, Gentry C, Vastani N, Sensi S, Bevan S, Goebel A et al (2019) Autoantibodies produce pain in complex regional pain syndrome by sensitizing nociceptors. Pain 160:2855–2865. https://doi.org/10.1097/j.pain.0000000000001662
12. Daifallah O, Farah A, Dawes JM (2023) A role for pathogenic autoantibodies in small fiber neuropathy? Front Mol Neurosci 16:1254854. https://doi.org/10.3389/fnmol.2023.1254854
13. Dawes JM, Weir GA, Middleton SJ, Patel R, Chisholm KI, Pettingill P et al (2018) Immune or genetic-mediated disruption of CASPR2 causes pain hypersensitivity due to enhanced primary afferent excitability. Neuron 97:806-822.e810. https://doi.org/10.1016/j.neuron.2018.01.033
14. Elboraay T, Ebada MA, Elsayed M, Aboeldahab HA, Salamah HM, Rageh O et al (2025) Long-term neurological and cognitive impact of COVID-19: a systematic review and meta-analysis in over 4 million patients. BMC Neurol 25(1):250. https://doi.org/10.1186/s12883-025-04174-9
15. Ely EW, Brown LM, Fineberg HV (2024) Long Covid defined. N Engl J Med 391:1746–1753. https://doi.org/10.1056/NEJMsb2408466
16. Franke C, Boesl F, Goereci Y, Gerhard A, Schweitzer F, Schroeder M et al (2023) Association of cerebrospinal fluid brain-binding autoantibodies with cognitive impairment in post-COVID-19 syndrome. Brain Behav Immun 109:139–143. https://doi.org/10.1016/j.bbi.2023.01.006
17. Franke C, Ferse C, Kreye J, Reincke SM, Sanchez-Sendin E, Rocco A et al (2021) High frequency of cerebrospinal fluid autoantibodies in COVID-19 patients with neurological symptoms. Brain Behav Immun 93:415–419. https://doi.org/10.1016/j.bbi.2020.12.022
18. Fujii T, Lee EJ, Miyachi Y, Yamasaki R, Lim YM, Iinuma K et al (2021) Antiplexin D1 antibodies relate to small fiber neuropathy and induce neuropathic pain in animals. Neurol Neuroimmunol Neuroinflamm 8:1028. https://doi.org/10.1212/nxi.0000000000001028
19. Getts DR, Chastain EM, Terry RL, Miller SD (2013) Virus infection, antiviral immunity, and autoimmunity. Immunol Rev 255:197–209. https://doi.org/10.1111/imr.12091
20. Goebel A, Krock E, Gentry C, Israel MR, Jurczak A, Urbina CM et al (2021) Passive transfer of fibromyalgia symptoms from patients to mice. J Clin Invest 131:144201. https://doi.org/10.1172/jci144201
21. Hamlin RE, Pienkos SM, Chan L, Stabile MA, Pinedo K, Rao M et al (2024) Sex differences and immune correlates of Long Covid development, symptom persistence, and resolution. Sci Transl Med 16:eadr1032. https://doi.org/10.1126/scitranslmed.adr1032
22. Helyes Z, Tékus V, Szentes N, Pohóczky K, Botz B, Kiss T et al (2019) Transfer of complex regional pain syndrome to mice via human autoantibodies is mediated by interleukin-1-induced mechanisms. Proc Natl Acad Sci U S A 116:13067–13076. https://doi.org/10.1073/pnas.1820168116
23. Herrero-Montes M, Fernández-de-Las-Peñas C, Ferrer-Pargada D, Tello-Mena S, Cancela-Cilleruelo I, Rodríguez-Jiménez J et al (2022) Prevalence of neuropathic component in post-COVID pain symptoms in previously hospitalized COVID-19 survivors. Int J Clin Pract 2022:3532917. https://doi.org/10.1155/2022/3532917
24. Hofmann S, Lucio M, Wallukat G, Hoffmanns J, Schröder T, Raith F et al (2025) Functional autoantibodies targeting G-Protein-Coupled Receptors and their clinical phenotype in patients with Long-COVID. Int J Mol Sci 26:6746. https://doi.org/10.3390/ijms26146746
25. Houen G, Trier NH (2020) Epstein-Barr virus and systemic autoimmune diseases. Front Immunol 11:587380. https://doi.org/10.3389/fimmu.2020.587380
26. Hussein HM, Rahal EA (2019) The role of viral infections in the development of autoimmune diseases. Crit Rev Microbiol 45:394–412. https://doi.org/10.1080/1040841x.2019.1614904
27. Jernbom AF, Skoglund L, Pin E, Sjöberg R, Tegel H, Hober S et al (2024) Prevalent and persistent new-onset autoantibodies in mild to severe COVID-19. Nat Commun 15:8941. https://doi.org/10.1038/s41467-024-53356-5
28. Jimenez-Andrade JM, Herrera MB, Ghilardi JR, Vardanyan M, Melemedjian OK, Mantyh PW (2008) Vascularization of the dorsal root ganglia and peripheral nerve of the mouse: implications for chemical-induced peripheral sensory neuropathies. Mol Pain 4:10. https://doi.org/10.1186/1744-8069-4-10
29. Kohr D, Singh P, Tschernatsch M, Kaps M, Pouokam E, Diener M et al (2011) Autoimmunity against the β2 adrenergic receptor and muscarinic-2 receptor in complex regional pain syndrome. Pain 152:2690–2700. https://doi.org/10.1016/j.pain.2011.06.012
30. Kubota GT, Soares FHC, da Fonseca AS, Rosa TDS, da Silva VA, Gouveia GR et al (2023) Pain paths among post-COVID-19 condition subjects: a prospective cross-sectional study with in-person evaluation. Eur J Pain 27:636–650. https://doi.org/10.1002/ejp.2094
31. Kubota T, Kuroda N, Sone D (2023) Neuropsychiatric aspects of long COVID: a comprehensive review. Psychiatry Clin Neurosci 77:84–93. https://doi.org/10.1111/pcn.13508
32. Lacagnina MJ, Heijnen CJ, Watkins LR, Grace PM (2021) Autoimmune regulation of chronic pain. PAIN Rep 6:e905. https://doi.org/10.1097/pr9.0000000000000905
33. Lacagnina MJ, Willcox KF, Boukelmoune N, Bavencoffe A, Sankaranarayanan I, Barratt DT et al (2024) B cells drive neuropathic pain-related behaviors in mice through IgG-Fc gamma receptor signaling. Sci Transl Med 16:eadj1277. https://doi.org/10.1126/scitranslmed.adj1277
34. Lavi Y, Vojdani A, Halpert G, Sharif K, Ostrinski Y, Zyskind I et al (2023) Dysregulated levels of circulating autoantibodies against neuronal and nervous system autoantigens in COVID-19

patients. Diagnostics Basel 13:687. https://doi.org/10.3390/diagnostics13040687
35. Lucchese G, Vogelgesang A, Boesl F, Raafat D, Holtfreter S, Bröker BM et al (2022) Anti-neuronal antibodies against brainstem antigens are associated with COVID-19. EBioMedicine 83:104211. https://doi.org/10.1016/j.ebiom.2022.104211
36. Cornillet EV M, Cantagrel A, Serre G, Nogueira L (2014) A6.6 In RA patients, antibodies to the citrullinated peptide EBNA35-58Cit from Epstein-Barr nuclear antigen-1 crossreact with the citrullinated fibrin peptide β60-74Cit60,72,74. Ann Rheum Dis 73:A73
37. McAlpine L, Zubair AS, Joseph P, Spudich S (2024) Case-Control Study of Individuals With Small Fiber Neuropathy After COVID-19. Neurol Neuroimmunol Neuroinflamm 11:e200244. https://doi.org/10.1212/nxi.0000000000200244
38. Moen JK, Baker CA, Iwasaki A (2025) Neuroimmune pathophysiology of long COVID. Psychiatry Clin Neurosci 79:514–530. https://doi.org/10.1111/pcn.13855
39. Morse BA, Motovilov K, Michael Brode W, Michael Tee F, Melamed E (2025) A review of intravenous immunoglobulin in the treatment of neuroimmune conditions, acute COVID-19 infection, and post-acute sequelae of COVID-19 syndrome. Brain Behav Immun 123:725–738. https://doi.org/10.1016/j.bbi.2024.10.006
40. Munir A, Khan S, Saleem A, Nusrat H, Khan SA, Sayyed H et al (2025) The Role of Epstein-Barr Virus Molecular Mimicry in Various Autoimmune Diseases. Scand J Immunol 101:e70016. https://doi.org/10.1111/sji.70016
41. Needham EJ, Ren AL, Digby RJ, Norton EJ, Ebrahimi S, Outtrim JG et al (2022) Brain injury in COVID-19 is associated with dysregulated innate and adaptive immune responses. Brain 145:4097–4107. https://doi.org/10.1093/brain/awac321
42. Oguz-Akarsu E, Gullu G, Kilic E, Dinç Y, Akdag G, Rehber C et al (2024) Beyond the acute: pain in long COVID survivors at 1.5 years. Neurol Sci 45:4109–4117. https://doi.org/10.1007/s10072-024-07620-7
43. Peluso MJ, Deeks SG (2024) Mechanisms of long COVID and the path toward therapeutics. Cell 187:5500–5529. https://doi.org/10.1016/j.cell.2024.07.054
44. Peng K, Li X, Yang D, Chan SCW, Zhou J, Wan EYF et al (2023) Risk of autoimmune diseases following COVID-19 and the potential protective effect from vaccination: a population-based cohort study. EClinicalMedicine 63:102154. https://doi.org/10.1016/j.eclinm.2023.102154
45. Premraj L, Kannapadi NV, Briggs J, Seal SM, Battaglini D, Fanning J et al (2022) Mid and long-term neurological and neuropsychiatric manifestations of post-COVID-19 syndrome: a meta-analysis. J Neurol Sci 434:120162. https://doi.org/10.1016/j.jns.2022.120162
46. Li JW Q, Niu L, Yang S, Liang C (2024) High sensitive detection and validation of neuronal specific autoantibodies in post COVID-19 patients with neurocognitive disorders. J Immunol 212:0146_4992. https://doi.org/10.4049/jimmunol.212.supp.0146.4992
47. Salih LY, Dumaire NLA, Gieré C, Vest E, Alkhateeb H, Moritz CP et al (2026) Pathogenic role of FGFR3 autoantibodies in small fiber neuropathy. Adv Sci. https://doi.org/10.1002/advs.202511413
48. Santos Guedes de Sa K, Silva J, Bayarri-Olmos R, Brinda R, Constable R AR, Diaz PA C et al (2024) A causal link between autoantibodies and neurological symptoms in Long COVID. medRxiv. https://doi.org/10.1101/2024.06.18.24309100
49. Seibert FS, Stervbo U, Wiemers L, Skrzypczyk S, Hogeweg M, Bertram S et al (2023) Severity of neurological Long-COVID symptoms correlates with increased level of autoantibodies targeting vasoregulatory and autonomic nervous system receptors. Autoimmun Rev 22:103445. https://doi.org/10.1016/j.autrev.2023.103445
50. Smatti MK, Cyprian FS, Nasrallah GK, Al Thani AA, Almishal RO, Yassine HM (2019) Viruses and autoimmunity: A review on the potential interaction and molecular mechanisms. Viruses 11:762. https://doi.org/10.3390/v11080762
51. Sundaresan B, Shirafkan F, Ripperger K, Rattay K (2023) The role of viral infections in the onset of autoimmune diseases. Viruses 15:782. https://doi.org/10.3390/v15030782
52. Syed U, Subramanian A, Wraith DC, Lord JM, McGee K, Ghokale K et al (2023) Incidence of immune-mediated inflammatory diseases following COVID-19: A matched cohort study in UK primary care. BMC Med 21:363. https://doi.org/10.1186/s12916-023-03049-5
53. Tabacof L, Chiplunkar M, Canori A, Howard R, Wood J, Proal A et al (2024) Distinguishing pain profiles among individuals with long COVID. Front Rehabil Sci 5:1448816. https://doi.org/10.3389/fresc.2024.1448816
54. Tesch F, Ehm F, Vivirito A, Wende D, Batram M, Loser F et al (2023) Incident autoimmune diseases in association with SARS-CoV-2 infection: a matched cohort study. Clin Rheumatol 42:2905–2914. https://doi.org/10.1007/s10067-023-06670-0
55. Tholance Y, Antoine JC, Mohr L, Jung M, Reynaud-Federspiel E, Ferraud K et al (2021) Anti-FGFR3 antibody epitopes are functional sites and correlate with the neuropathy pattern. J Neuroimmunol 361:577757. https://doi.org/10.1016/j.jneuroim.2021.577757
56. Thompson JS, Thornton AC, Ainger T, Garvy BA (2022) Long-term high-dose immunoglobulin successfully treats Long COVID patients with pulmonary, neurologic, and cardiologic symptoms. Front Immunol 13:1033651. https://doi.org/10.3389/fimmu.2022.1033651
57. Valadez-Calderon J, Ordinola Navarro A, Rodriguez-Chavez E, Vera-Lastra O (2022) Co-expression of anti-NMDAR and anti-GAD65 antibodies. A case of autoimmune encephalitis in a post-COVID-19 patient. Neurologia (Engl Ed) 37:503–504. https://doi.org/10.1016/j.nrleng.2021.09.004
58. Visvabharathy L, Dalil N, Leonor L, Zhu C, Orban ZS, Jimenez M et al (2024) Mild primary or breakthrough SARS-CoV-2 infection promotes autoantibody production in individuals with and without Neuro-PASC. Immunohorizons 8:577–585. https://doi.org/10.4049/immunohorizons.2400033
59. Wallukat G, Hohberger B, Wenzel K, Fürst J, Schulze-Rothe S, Wallukat A et al (2021) Functional autoantibodies against G-protein coupled receptors in patients with persistent Long-COVID-19 symptoms. J Transl Autoimmun 4:100100. https://doi.org/10.1016/j.jtauto.2021.100100
60. Wang EY, Mao T, Klein J, Dai Y, Huck JD, Jaycox JR et al (2021) Diverse functional autoantibodies in patients with COVID-19. Nature 595:283–288. https://doi.org/10.1038/s41586-021-03631-y

Authors and Affiliations

Margaux Mignolet[1] · Catherine Deroux[2] · Thomas Florkin[1] · Valéry Bielarz[1] · Kathleen De Swert[1] · Nicolas Halloin[1] · Lindsay Sprimont[1] · Aurélie Ladang[3] · Fabienne George[4,5] · Jacques Gilloteaux[1,6] · Laurence Abeloos[7] · Pierre Garin[8,9] · Johan Van Weyenbergh[10] · Marc Jamoulle[11] · Claire Diederich[12] · Nicolas Albert Gillet[12] · Pierre Bulpa[5,13] · Charles Nicaise[1]

✉ Charles Nicaise
charles.nicaise@unamur.be

[1] URPhyM, NARILIS, Université de Namur, Namur, Belgium

[2] Clinique de La Mémoire, Service de Neurologie, CHU-UCL Namur, Site Godinne, Yvoir, Belgium

[3] Laboratoire de Chimie Clinique, CHU Liège, Liège, Belgium

[4] Biobanque, CHU-UCL Namur, Site Godinne, Yvoir, Belgium

[5] NARILIS, CHU-UCL Namur, Namur, Belgium

[6] Department of Anatomical Sciences, St George's University School of Medicine, Newcastle Upon Tyne, UK

[7] Centre de La Douleur Chronique, Grand Hôpital de Charleroi, Charleroi, Belgium

[8] Laboratoire d'Anatomie, Université de Namur, Namur, Belgium

[9] Oto-Rhino-Laryngologie, Mont-Godinne University Hospital, CHU-UCL Namur, Site Godinne, Yvoir, Belgium

[10] Rega Institute, KULeuven, Leuven, Belgium

[11] HEC Information Sciences, Université de Liège, Liège, Belgium

[12] URVI, NARILIS, Université de Namur, Namur, Belgium

[13] Intensive Care Unit, CHU-UCL Namur, Site Godinne, Yvoir, Belgium